

Copyright  
by  
Angel Rualdo Soto Chavez  
2010

The Dissertation Committee for Angel Rualdo Soto Chavez  
certifies that this is the approved version of the following dissertation:

## **Relativistic Wave Phenomena in Astrophysical Plasmas**

Committee:

---

Swadesh M. Mahajan, Supervisor

---

Richard D. Hazeltine, Supervisor

---

Boris Breizman

---

Duane A. Dicus

---

Irene Gamba

# Relativistic Wave Phenomena in Astrophysical Plasmas

by

Angel Rualdo Soto Chavez, B.S., Diploma

## DISSERTATION

Presented to the Faculty of the Graduate School of  
The University of Texas at Austin  
in Partial Fulfillment  
of the Requirements  
for the Degree of

## DOCTOR OF PHILOSOPHY

THE UNIVERSITY OF TEXAS AT AUSTIN

May 2010

To my son Leonardo. I hope that this work, and what it means, motivates you to achieve your own goals that, with effort and devotion, you will always accomplish.

*A mi hijo Leonardo. Espero que este trabajo, y lo que significa, te motive para que alcances tus propias metas que, con mucho esfuerzo y dedicacion, siempre cumpliras.*

## Acknowledgments

I want to thank my supervisors: Swadesh Mahajan and Richard Hazeltine. To Swadesh for giving me the opportunity to work on what I always wanted. To Richard for his support (and for having me at the blackboard every time I had to explain him something). Most importantly, I want to thank you both for the long and valuable discussions we had, I learned much from you. I want to thank the Institute for Fusion Studies' scientists, staff and students. Particularly: Herb Berk, Boris Breizman, James VanDam and Cathy Rapinett. I want to thank the Physics Department of The University of Texas at Austin for accepting me as a graduate student. I want to thank also the dissertation Committee. I also want to thank Melvin Oakes and the family Little: Scott, Stephanie, Betty for their hospitality and of course for the Robert N. Little fellowship that provided me so much relief in this hard economic times. Without them my life here in the US would have been much harder. To Fernando Quevedo for his support, before and during, my studies here in Texas and in Italy, I have much to thank him. To my friends in this long journey here at Texas: Nacho, Rodolfo, Marcus, Erick, Rongfeng, Donna, Ema, Jessa, Maria. To my former professor Rodolfo Samayoa who was my mentor during my studies in Guatemala, I owe him a lot. As always this work would not have been possible without the support, and encouragement, of my parents: Rualdo and Blanca. To my sisters: Susy and Blanquita

who I miss so much during this time outside my home country. To all my nephews and nieces. To all my cousins, aunts, uncles, brothers in law, parents in law and my grandparents: Gloria, Graciela<sup>‡</sup>, Clementino and Angel, thank you all.

And last, I want to thank specially to you my dear love, Lorena, for making this journey as a PhD student worthwhile and for being by my side, in good and bad times, all these years. Without you I just simple would not have done it.

# Relativistic Wave Phenomena in Astrophysical Plasmas

Publication No. \_\_\_\_\_

Angel Rualdo Soto Chavez, Ph.D.  
The University of Texas at Austin, 2010

Supervisors: Swadesh M. Mahajan  
Richard D. Hazeltine

The propagation and stability of waves in relativistic astrophysical plasmas is presented. Our investigation, using a relativistic two-fluid model, is different from previous relativistic fluid studies in that the plasma is treated fully relativistically, both in temperature and in directed speed. Much of this study is devoted to relativistic linear waves in pulsar pair plasmas, with a view to elucidating a possible mechanism for pulsar radio wave emission. We also study interesting nonlinear exact solutions in both relativistic and non-relativistic plasmas.

Pulsar pair plasmas can support four transverse modes for parallel propagation. Two of these are electromagnetic plasma modes, which at high temperature become light waves. The remaining two are Alfvénic modes, split into a fast and a slow mode. The slow mode, always sub-luminous, is cyclotron (Alfvén) two-stream unstable at large wavelengths. We find that temperature effects, within the fluid model used, do not suppress the instability in the limit

of large (finite) magnetic field. The fast Alfvén mode can be super-luminous only at large wavelengths; however, it is always sub-luminous at high temperatures. In this incompressible approximation, only the ordinary mode is present for perpendicular propagation.

We discuss the implications of the unstable mode for radio emission mechanisms. For typical values, the instability is quite fast, and the waves can grow to sizable levels, such that, the magnetic modulation could act as a wiggler. The pulsar primary beam interacting with this wiggler, could drive a free electron laser (FEL) effect, yielding coherent radiation. Investigation of the FEL in this setting and demonstrating that the frequency spectral range, and luminosities, predicted by this mechanism is well within the observed range of radio frequency (and luminosity) emissions, is one of the principal results of this dissertation. It is tempting to speculate, then, that an FEL-like radiation effect could be responsible for the highly coherent radio wave emissions from pulsars.

In the study of nonlinear exact solutions we have generalized the results to the incompressible Hall Magnetohydrodynamics (HMHD). We find that for cases when the plasma is weakly magnetized ( $V_A \ll c$ ) the frequencies of the modes decrease as the wave amplitude (effective mass) increases. For very strongly magnetized plasmas the light-like modes tend to be asymptotically linear; the frequency is unaffected by wave amplitude.

# Table of Contents

<b>Acknowledgments</b>	<b>v</b>
<b>Abstract</b>	<b>vii</b>
<b>List of Figures</b>	<b>xii</b>
<b>Chapter 1. Introduction</b>	<b>1</b>
1.1 Pulsars . . . . .	4
1.1.1 Pulsar properties . . . . .	7
1.1.2 Observational features . . . . .	10
<b>Chapter 2. Model</b>	<b>15</b>
<b>Chapter 3. Physics of Pulsars Magnetospheres</b>	<b>19</b>
3.1 Introduction . . . . .	19
3.2 Pulsar magnetosphere: standard model . . . . .	20
3.2.1 Polar cap model . . . . .	24
3.2.2 Pair ( $e^-$ , $e^+$ ) plasmas . . . . .	26
<b>Chapter 4. Relativistic Waves in Pulsar Plasmas</b>	<b>30</b>
4.1 Introduction . . . . .	30
4.1.1 Basic concepts . . . . .	31
4.2 Linear waves in pulsars . . . . .	33
4.2.1 Waves propagating parallel ( $\mathbf{k} \parallel \hat{\mathbf{z}}$ ) . . . . .	37
4.2.1.1 Free energy source . . . . .	44
4.2.1.2 Zero streaming limit ( $V_o \rightarrow 0$ ) . . . . .	45
4.2.2 Waves propagating perpendicular ( $\mathbf{k} \perp \hat{\mathbf{z}}$ ) . . . . .	46
4.2.3 Waves propagating oblique ( $\theta = \pi/4$ ) . . . . .	48
4.2.4 Super strong magnetic field . . . . .	50

4.3	Numerical estimates . . . . .	53
4.4	Summary and conclusions . . . . .	56
<b>Chapter 5. Free Electron Lasers in Pulsar Magnetospheres</b>		<b>58</b>
5.1	Introduction . . . . .	58
5.2	Pulsar's radiation . . . . .	59
5.2.1	Coherence . . . . .	61
5.3	Free electron lasers . . . . .	62
5.3.1	Operating principle . . . . .	62
5.3.2	Electron motion in an undulator . . . . .	64
5.3.3	Energy exchange and condition for resonant interaction	68
5.3.4	Gain and electron beam requirements . . . . .	71
5.4	FEL in pulsar magnetospheres . . . . .	72
5.4.1	Frequency . . . . .	74
5.4.2	Power . . . . .	75
5.5	Discussion . . . . .	77
<b>Chapter 6. Exact solutions: nonlinear waves</b>		<b>78</b>
6.1	Introduction . . . . .	78
6.2	Relativistic nonlinear two-fluid waves . . . . .	79
6.3	Solution to the nonlinear equations . . . . .	82
6.3.1	Different species $\mu_+ \rightarrow 1, \mu_- \rightarrow 0$ . . . . .	83
6.3.1.1	Non-relativistic case ( $A_{\pm}^2 \ll 1$ ) . . . . .	83
6.3.1.2	Relativistic case ( $A_+^2 \lesssim 1$ ) . . . . .	85
6.3.1.3	$V_A \gg c$ . . . . .	88
6.3.2	Same species $\mu_+ = \mu_- \rightarrow 1/2$ . . . . .	89
6.3.2.1	Non-relativistic case ( $A_+^2 \ll 1$ ) . . . . .	90
6.3.2.2	Relativistic case ( $A_+^2 \lesssim 1$ ) . . . . .	91
6.3.2.3	Case $V_A \gg c$ . . . . .	92
6.4	Conclusions . . . . .	93
<b>Chapter 7. Summary</b>		<b>95</b>

<b>Appendix</b>	<b>98</b>
<b>Bibliography</b>	<b>102</b>
<b>Index</b>	<b>105</b>
<b>Vita</b>	<b>106</b>

## List of Figures

1.1	A 22 s time series from the Arecibo radio telescope showing single pulses from a typical pulsar. Insets show expanded views of selected pulses. Taken from “Handbook of Pulsar Astronomy”.	11
1.2	Integrated pulse profiles from a sample of nine pulsars. Taken from “Handbook of Pulsar Astronomy”.	12
1.3	Sample flux density spectra for two pulsars showing different types of spectral behavior. Taken from “Handbook of Pulsar Astronomy”.	14
3.1	Pulsar magnetosphere.	23
3.2	Polar Cap Region.	25
3.3	Pair production at the poles of neutron stars.	27
4.1	Dispersion curves for exactly parallel propagation ( $T \ll m_o$ ). There are four modes, the intermediate-dashed line is the vacuum dispersion $\omega = kc$ . For the slow Alfvén mode (thick solid line) $k < 2/V_o\gamma_o$ denotes the region of the cyclotron two-stream instability. The EMP modes (long and short dashed lines) have cutoff at $\omega = \sqrt{4\omega_p^2/G + 4\omega_c^2/G^2\gamma_o^2}$ . The point $k > 2\sqrt{\gamma_o^2 - 1}$ is where the fast Alfvén mode (continues line) becomes subluminal. The numerical parameters $\gamma_o = 1.3$ , $d = 1.5$ where chosen for the sake of graphical clarity.	39
4.2	Dispersion curves for parallel propagation, for temperatures $T = m_o$ ( $G = 4.37$ ). The labeling is the same used in Fig. 4.1. Note that, at short $k$ , the degeneracy of the EMP modes is still present, and the slow Alfvén wave is still unstable.	40
4.3	Dispersion curves for parallel propagation, for still higher temperatures $T > m_o$ . The labeling is the same used in Fig. 4.1. Note that the EMP modes have virtually become light waves.	41

4.4	Dispersion curves for exactly parallel propagation with ratio $4\gamma_o^2 V_o^2/d^2 < 1$ . Note that, as explained in text, the slow Alfvén wave (thick solid line) is unstable in two regions: $0 < k < k_- \approx 0.53$ and $k_+ \approx 1.87 < k < k_c \approx 2.41$ . The labeling for the rest of the curves is the same used in Fig. 4.1. The numerical parameters $\gamma_o = 1.3, d = 2$ where chosen for the sake of graphical clarity. . . . .	42
4.5	Numerical growth rate curves of the slow Alfvén mode, for various temperatures. Limit $d^2/\gamma_o^2 \gg V_o^2\gamma_o^2$ . Note that, as explained in the text, for temperatures of the order of $T \sim m_o$ the instability is not completely suppressed. With numerical parameters $\gamma_o = 1.3, d = 4$ . . . . .	44
4.6	Dispersion curves for zero streaming ( $\gamma_o = 1, d = 1$ ). For temperatures: $T \ll m_o$ (continues lines) and $T = m_o$ (dashed lines). Notice the lowered cutoff of the EMP modes, and the frequency drop for the Alfvénic mode at $T = m_o$ . . . . .	46
4.7	Dispersion curves for perpendicular propagation ( $\theta = \pi/2, d = 1$ ). Note how the increasing of temperature lowers the plasma cutoff until it reaches the asymptotic $kc$ limit. . . . .	48
4.8	Dispersion curves for oblique propagation. Here we have four modes, two of them are EMP modes (short and long dashed lines). The slow branches (continues and thick lines) are the fast and slow Alfvénic modes respectively. Cold plasma ( $T \ll m_o$ ), $\gamma_o = 1.3, d = 2$ . . . . .	49
4.9	Dispersion curves for oblique propagation, for high temperatures $T > m_o$ ( $\gamma_o = 1.3, d = 1.5$ ). Labeling same as in Fig. 4.8. . . . .	50
4.10	Dispersion curves for Parallel propagation. Super strong B field, cold plasma. The fast EMP mode (short dashed line) have dispersion $\omega \approx 2/\gamma_o + V_o k$ . The slow Alfvén mode (thick solid line) is divided in three regions. The slow EMP (long dashed line) and fast Alfvén modes (continues line) have dispersion relations as described in the text. The numerical parameters $\gamma_o = 4, d = 10^5$ were chosen for the sake of graphical clarity. . . . .	52
4.11	Dispersion curves for Parallel propagation. Strong B field. For $T = m_o, \gamma_o = 4, d = 10^5$ . Notice the increase of temperature manifested through the decreasing cutoffs, making the curves approach the line $kc$ . Labeling same as in Fig. 4.10. . . . .	53
4.12	Dispersion for parallel propagation, for still higher temperatures $T > m_o$ . Strong B field. Still $\gamma_o = 4, d = 10^5$ . Here the cutoffs $\pm 2/[\gamma_o G(T)]$ , have become approximately zero and the curves have become virtually the line $k$ . Labeling same as in Fig. 4.10. . . . .	54

4.13	Dispersion curves for Oblique propagation. Strong B field. The EMP modes (long dashed line) have become asymptoted to $kc$ . The Alfvénic modes (continues and thick lines) have become asymptoted to $kc/\sqrt{2}$ (short dashed line). With $\gamma_o = 10, d = 10^5$ .	55
5.1	Sphere of radius R, at a distance d	60
5.2	Free electron laser. The electron motion is on a plane perpendicular to the magnetic field lines.	63
5.3	FEL, Optical cavity.	64
5.4	FEL SASE	65
5.5	Schematic picture: electron motion in undulator	66
5.6	FEL saturation. The power depends linearly on the input power (exponential regime). However the saturation power is independent on the input power. Taken from “FEL Theory for Pedestrians” by Peter Schmuser.	73
6.1	Dispersion curves: non-relativistic case ( $V_A \ll c$ ). Note the cyclotron branch (large $k$ ) asymptotic to 1, or $\omega_c$ in physical units.	85
6.2	Dispersion curves: relativistic case. Alfvénic modes, for various amplitudes $A_+$ , with $\hat{e}_s \cdot \hat{e}_z = -1$ .	86
6.3	Whistler mode for various amplitudes $A_-$ .	87
6.4	Vacuum dispersion relations for different velocity amplitudes ( $V_A \gg c$ ).	89
6.5	Alfvénic modes in pair plasmas, note the asymptotic limit of 2, at large $k$ .	90
6.6	Electromagnetic plasma modes for various velocity amplitudes.	92
6.7	Vacuum dispersion relation in pair plasma, limit $V_A \gg c$ . Note that the curve is unaffected by the increasing amplitude $A_+$ .	93

# Chapter 1

## Introduction

The present work deals with wave propagation in astrophysical plasmas. The plasma state is categorized by the fundamental plasma parameters: density  $n$ , temperature  $T$ , magnetic field  $B$ , and the derived parameters: plasma frequency  $\omega_p$ , cyclotron frequency  $\omega_c$ , thermal velocity  $v_{th}$ , etc. In astrophysical plasmas these parameters cover such a wide range of values that it is difficult to establish a good definition for astrophysical plasmas.

Additionally, in some astrophysical settings, such as jets, accretion disks surrounding compact objects and pulsar magnetospheres, the plasma is often relativistic. A plasma is considered relativistic [1] when one or both of the following is true. (1) The bulk velocity of the plasma  $V$  is close to the speed of light  $c$ , that is,  $V \sim c$ . (2) Its random energy (temperature) is of the order (or larger) of the rest mass energy of the particles that form it, that is,  $T \sim mc^2/k_B$ .

It is well known that the plasma state is rich in the different types of waves that it can support.

Studies of wave propagation in plasmas have been an active field ever since plasmas were discovered. The first studies began with Langmuir in the

1920's, when he identified certain phenomena with wave motions in arc discharges. In 1929, Tonks and Langmuir [2] presented the theory of these waves. Their studies focused on unmagnetized plasmas. Just after their work, Hartree in 1931 [3] and Appleton in 1932 [4] studied radio wave propagation in the ionosphere, which led to the magnetoionic theory. In 1942, Alfvén [5], motivated by astrophysical implications, studied waves in magnetized plasmas. He modeled the plasma as a highly conductive and incompressible fluid. During the 1940's and 1950's, the kinetic theory of plasmas was developed. One of the most important aspects studied during this time was plasma instabilities, which involves waves in some exponentially growing mode.

During these years, and after the second World War, the study of astrophysical phenomena was boosted, mainly, by the invention of the radar. Astronomers were pointing radio telescopes to the sky in search for signals that could be analyzed and identified. Among others, one of the most important discoveries was that of radio pulses emitted by pulsars.

After the discovery of pulsars, physicists and astronomers alike embarked on a quest to study what a pulsar was and how the pulsar's radio pulses were created. It was soon realized that pulsars were neutron stars and the pulses were being generated in the star's atmosphere, now called the magnetosphere.

Understanding how the magnetosphere works, and the type of waves that it can support, was crucial in developing a theoretical model that could explain those pulses.

As we will explain in Chapter 3, pulsar plasmas are composed of two main ingredients: a relativistic charged primary beam and the secondary relativistic beams. The secondary relativistic beams are basically composed of electrons ( $e^-$ ) and positrons ( $e^+$ ). Such plasmas are sometimes called pair plasmas.

The study of wave propagation in pulsar plasmas has, therefore, focused on understanding the propagating modes in magnetized pair plasmas. Also, one of the aims is to understand the instabilities generated under the pulsars' magnetospheric conditions. The inclusion of temperature has also been one of the biggest concerns, and one of the greatest challenges as well [6], because many of the instabilities found were thought to be suppressed at high temperatures, even though the actual temperatures of pulsar pair plasmas was not known. Until recently [7], it was shown that the  $e^-e^+$  distribution function of such plasmas is likely to be Maxwellian with temperatures very close to  $T \sim m_o c^2/k_B$ , i.e., the average random energy is of the order of the rest mass.

Therefore we face the following problem: much of the existent literature on modes (see, e.g., [6, 8, 9, 10, 11, 12], and references therein) and instabilities employ relativistic cold fluid models (see, e.g., [9]). Even in kinetic theory treatments, analytically convenient particle distribution functions (such as waterbag) were assumed to derive dispersion relations, without much physical justifications [8, 12]. When more appropriate distributions (such as the Maxwellian) are investigated [11], the range of temperatures is restricted (too low,  $T \ll mc^2/k_B$ , or too high,  $T \gg mc^2/k_B$ ).

In this work, we study wave propagation and dispersion relations in astrophysical plasmas. This work is novel because we analyze the temperature effects, at  $T \sim mc^2/k_B$ , on propagating waves in pulsar pair plasmas (see Chapter 4). For this, we use (see Chapter 2) a fully relativistic fluid model: relativistic in both temperature and directed speed.

We find (see Chapter 4) that even in the range of temperatures relevant to pulsar magnetospheres, the instabilities are not suppressed. This important result has lead us to investigate a mechanism that could possible explain the main features of the pulsars' radio emissions: see Chapter 5.

Last, in Chapter 6, we study nonlinear waves in cold relativistic plasmas. These non-linear waves, could help explain some of the properties seen in turbulent space plasmas.

We will now briefly describe some of the physical and observational properties of pulsars; these properties will be needed throughout this text.

## 1.1 Pulsars

The history of pulsars dates back to the year 1967. In that year, Jocelyn Bell, a young graduate student, discovered a series of radio pulses [13] using a radio antenna designed by her thesis supervisor, Antony Hewish. (For a complete review, of this remarkable discovery see, for example, [14]). The intensity of such radio pulses varied over a wide range in strength, but, they had the remarkable property of being periodic. The precision of the periodicity

of the pulses is such that it has been compared with that of atomic clocks. Because of this, and the later identification of the phenomenon with neutron stars, they were coined pulsars for “pulsating stars.”

The identification with neutron stars was not straightforward. Orbital motion and rotation were among the several mechanisms proposed to explain the pulses. The earliest studies of neutron stars, including studies by their discoverers, speculated about dwarf stars and even planetary binary systems. One of the main barriers for their association with neutron stars was that neutron stars were a field of study only familiar to certain theoretical astrophysicists, who were primarily concerned with different states of matter and their implications to the surrounding gravitational field as precursors to black holes.

The possibility that a pulsar was a planet (or some kind of a satellite) orbiting a massive star was ruled out by Ostriker in 1968, due to concerns about gravitational radiation [15]. The energy losses through this radiation would imply a fast decrease in orbital period, something that was not in accord with the pulse’s periodicity. Early reports showed that the basic periodicities of pulsars were stable to a precision better than one part in  $10^7$  per year. There was the added problem that the planet would be disrupted by tidal forces.

The short periods, from milliseconds to a few seconds, showed that the objects producing the pulses must also be very compact compared to normal stellar objects. Dwarf stars were obvious candidates. Rotating white dwarfs, for example, are expected to be stable for rotation periods of a few seconds or

more, but with shorter periods, such as the ones found in most pulsars, they would be destroyed by centrifugal forces, as shown below.

The centrifugal force of a spinning star can be determined by assuming that the star is spherical, has an uniform density  $\rho$  with radius  $r$  and angular velocity  $w$ . The centrifugal force on a mass at its equator can be balanced by the gravitational force

$$\begin{aligned} mw^2r &= \frac{GMm}{r^2} \\ &= \frac{Gm}{r^2} \frac{4\pi}{3} \rho r^3. \end{aligned} \tag{1.1}$$

Therefore, the density is ( $w = 2\pi/P$ )

$$\rho = \frac{3\pi}{GP^2}. \tag{1.2}$$

For example, periods of  $P = 1$  s require densities greater than  $10^8 \text{ g cm}^{-3}$  which is just within the density range of a white dwarf star. However, for periods as short as 1 ms, much higher densities  $\sim 10^{14} \text{ g cm}^{-3}$ , such as those of neutrons stars, are required. The other impossibility of the dwarf star theory is that it is made of material that will eventually form a disk-like equatorial region, destroying the star.

Therefore, the fast-spinning neutron star model, first considered by Pacini (1967) [16] and Gold (1968) [17], was the simplest method of obtaining periods in the observed range. Further, some of the fast rotating pulsars are known to coincide with supernova remnants, and it was suggested long before that neutron stars would be formed in supernova explosions.

Thus, it had become quite evident that the neutron star model was superior. It was also clear that the neutron star model had to involve a type of “lighthouse effect”, where the emission beam sweeps past our line of sight once per rotation. However, the mechanism responsible for producing the pulses remained, and still remains, the most difficult to understand.

As we will show in Chapter 3, the radiation beam is, probably, emitted from the poles of the neutron star, where the conditions surrounding it, such as its magnetosphere, play a key role. The apparent brightness temperatures associated with the emitted radio pulses are such that the emission mechanism must be highly coherent, as we will explain it in Chapter 5.

### 1.1.1 Pulsar properties

The physical conditions inside a neutron star are very different from other types of stars. The average density is approximately  $\sim 10^{14} - 10^{15} \text{ g cm}^{-3}$ , these densities are even larger than that of nuclear matter. Its composition was first studied by Baade and Zwicky in 1934 [18] and Oppenheimer and Volkov in 1939 [19]. It is probable (see, e.g., [20]), that the star’s surface is composed of a solid crust made of iron nuclei and a sea of electrons with densities  $\rho \sim 10^6 \text{ g cm}^{-3}$ . Going inward, the density increases more, to a point where protons and electrons fuse to form neutrons, creating the neutron-rich nuclei of the inner crust. Deep into the star, the crust dissolves fully at  $\rho \sim 2 \times 10^{14} \text{ g cm}^{-3}$ , where the largest part of the neutron star is made up of a sea of free, superfluid neutrons.

Theoretical calculations of this highly compressed matter in a form of equation of state, predict [20] a maximum neutron star mass of about  $2M_s$ , where  $M_s \approx 2 \times 10^{33}$  g is the solar mass. Observational measurements of binary pulsars [21] are consistent with a typical pulsar mass of  $1.5M_s$  [20].

The associated moment of inertia  $I = kMR^2$ , where  $k = 2/5$  for a sphere of uniform density gives  $I \sim 10^{45}$  g cm<sup>2</sup> for a star of radius  $R = 10$  Km and  $M = 1.5M_s$ .

The pulsar's pulsed periods are observed to increase with time. The spin-down in pulsars are thought to be due to loss of rotational kinetic energy via ejected particles and electromagnetic radiation at the rotation frequency. The increasing rate  $\dot{P} \equiv dP/dt$  can be associated to the rate of loss of rotational kinetic energy by

$$\dot{E} = -\frac{d}{dt} \left( \frac{I\omega^2}{2} \right) = -I\omega\dot{\omega} = 4\pi^2 I \dot{P} P^{-3}, \quad (1.3)$$

the quantity  $\dot{E}$  is called spin-down energy and it represents the total output power by the neutron star. For a neutron star with  $I = 10^{45}$  g cm<sup>2</sup>, Eq. (1.3) gives

$$\dot{E} \approx 4 \times 10^{31} \text{ erg s}^{-1} \left( \frac{\dot{P}}{10^{-15}} \right) \left( \frac{P}{s} \right)^{-3}. \quad (1.4)$$

Where, for a “normal” pulsar,  $P = 0.2 - 0.5$  s and  $\dot{P} \sim 10^{-15}$  s s<sup>-1</sup>. For “millisecond” pulsars, however,  $P \sim 3$  ms and  $\dot{P} \sim 10^{-20}$  s s<sup>-1</sup>.

The estimates for age and magnetic field of pulsars are based on the assumption that the neutron star is in a vacuum. This is, as we will show in

Chapter 3, very unlikely. Therefore, the following numerical estimates should be interpreted with some care.

The radiation power emitted by a rotating magnetic dipole with moment  $|\mathbf{m}|$  is given by [22]

$$P_r = \frac{2}{3c^3} |\mathbf{m}|^2 \omega^4 \sin^2 \theta, \quad (1.5)$$

where  $\theta$  is the angle between the magnetic moment and the spin axis. By equating  $P_r$ , with Eq. (1.3), one can derive the rotational frequency evolution

$$\dot{w} = - \left( \frac{2|\mathbf{m}|^2 \sin^2 \theta}{3c^3 I} \right) w^3, \quad (1.6)$$

or it can also be expressed as a power law ( $w = 2\pi/P$ )

$$\dot{P} = K P^{2-n}, \quad (1.7)$$

where  $n = 3$  is for a pure magnetic dipole and  $K$  is taken to be a constant. Values of  $n$ , for typical pulsars vary from  $n = 1.4$  to  $n = 2.9$  [21].

The pulsar's magnetic field strength ( $B$ ) can be estimated from Eq. (1.6), since the magnetic moment is related to  $B = |\mathbf{m}|/r^3$ , so

$$B_o \equiv B_{r=R} = \left( \frac{3c^3 I \dot{P} P}{8\pi^2 R^6 \sin^2 \theta} \right)^{1/2}, \quad (1.8)$$

$$B_o \approx 10^{12} \text{ G} \left( \frac{\dot{P}}{10^{-15}} \right)^{1/2} \left( \frac{P}{s} \right)^{1/2} \quad (1.9)$$

where  $R = 10 \text{ km}$ ,  $\sin \theta = 1$  and  $I = 10^{45} \text{ g cm}^2$ . Last, the characteristic age of the pulsar can be estimated to be [23]

$$t_c = \frac{P}{2\dot{P}} \sim 16 \text{ Myr} \left( \frac{\dot{P}}{10^{-15}} \right)^{-1} \left( \frac{P}{s} \right). \quad (1.10)$$

### 1.1.2 Observational features

Forty three years later, the observational characteristics of pulsars are now well established. However, the mechanism that produces the radio pulses is still not understood, despite much work and effort to explain it.

Here we will summarize the most important aspects. For a complete review, see, for example, [14]. At present roughly 1600 pulsars are known. Figure 1.1 demonstrates the basic pulsar signal, where intensity is plotted as a function of time. As we have seen above, the standard interpretation is that these pulses are produced by a lighthouse effect. Regardless of the pulse intensity, the basic timing of pulses is periodic. If the resolution time is reduced to the order of milliseconds, a more complex pulse structure is revealed. Individual pulses are found to consist of two or more subpulses; despite this, the shape of the integrated profile is quite stable. An integrated pulse profile is the addition of many hundreds of pulses together, a process known as folding, see Fig. 1.2.

Although the majority of pulsars discovered emit in the radio frequency band, they have also been detected in the optical, X-ray and gamma-ray frequencies. In general the radio-frequency flux density is given by the following power law

$$F \propto \nu^\alpha \tag{1.11}$$

where  $F$  is the flux density (see Chapter 5),  $\nu$  is the frequency and  $\alpha$  is the spectral index. The observed range of spectral indices is broad ( $-4 \lesssim \alpha \lesssim 0$ )

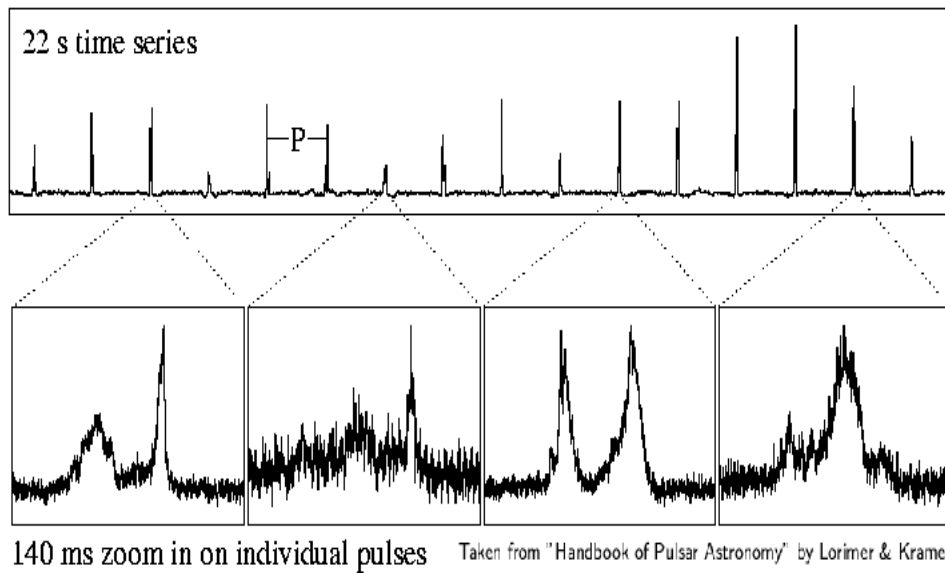


Figure 1.1: A 22 s time series from the Arecibo radio telescope showing single pulses from a typical pulsar. Insets show expanded views of selected pulses. Taken from “Handbook of Pulsar Astronomy”.

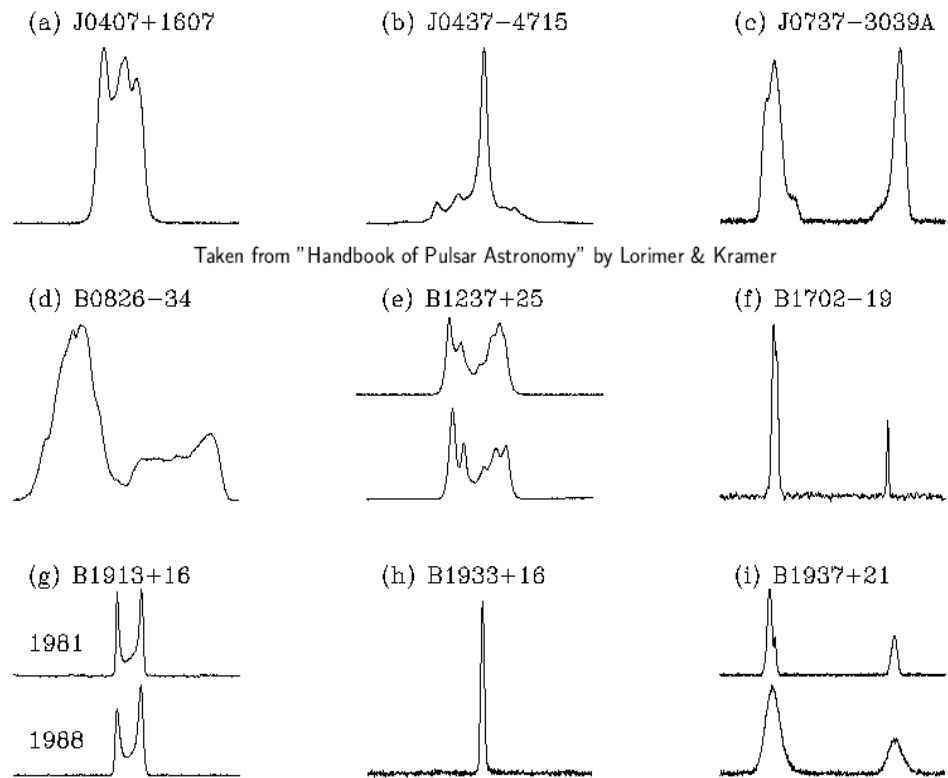


Figure 1.2: Integrated pulse profiles from a sample of nine pulsars. Taken from "Handbook of Pulsar Astronomy".

with a mean of  $-1.8 \pm 0.2$ , see Fig. 1.3. For a pulsar at distance  $d$ , the luminosity is given by [21]

$$L \sim 10^{27} \text{ erg s}^{-1} \left( \frac{F_{1400}}{\text{mJy}} \right) \left( \frac{d}{\text{kpc}} \right)^2, \quad (1.12)$$

where  $F_{1400}$  is the mean flux density at 1.4 GHz. Typical pulsar luminosities vary from  $10^{25}$  to  $10^{28}$  erg s $^{-1}$ . The brightness temperatures, corresponding to these fluxes and luminosities, are extremely large. The brightness temperature (see Chapter 5) corresponds to the temperature of a black body radiating the same observed radio intensity. Typical values are in the range of  $10^{23}$  to  $10^{31}$  K.

Therefore any radio emission theory must be capable of explaining radio broadband emission, at both radio and optical frequencies, and the high brightness temperatures associated with the corresponding luminosities. As we will show in Chapter 5, our proposed model gives the correct expected frequencies and luminosities.

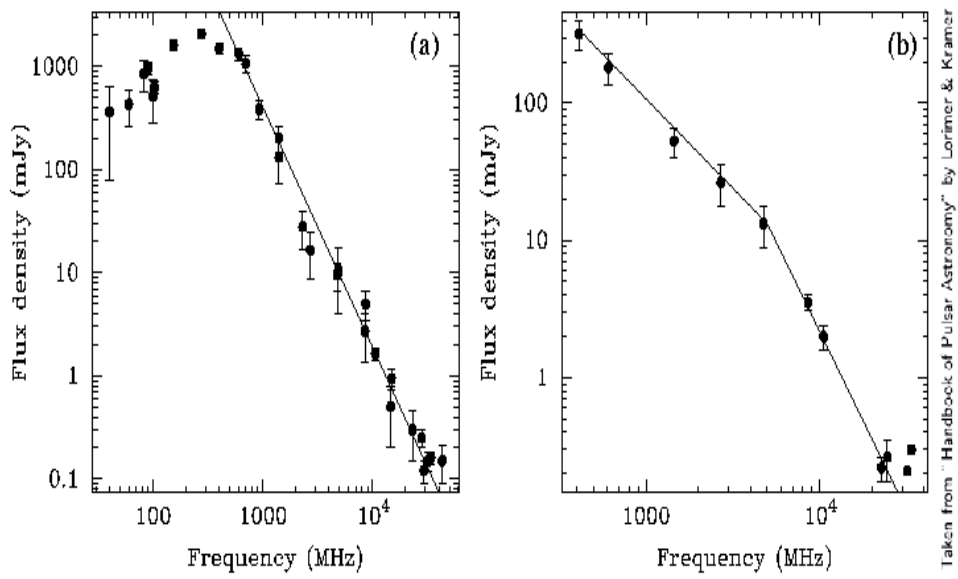


Figure 1.3: Sample flux density spectra for two pulsars showing different types of spectral behavior. Taken from “Handbook of Pulsar Astronomy”.

## Chapter 2

### Model

In this chapter we will introduce the relativistic fluid model to be used. This fluid model is derived by assuming that the particles' distribution function ( $f$ ) is a local relativistic Maxwellian, that is

$$f_s = \frac{n_R z_s}{4\pi K_2(z_s)} \exp[-\mathcal{E}_s/T_s], \quad (2.1)$$

where  $\mathcal{E} = \sqrt{m^2 c^4 + P^2 c^2}$  and  $T$  are, respectively, the energy and temperature of the species  $s$ . In our units, the Boltzmann's constant ( $k_B$ ) is set to one ( $k_B = 1$ ). Then the dynamics of such particles are described by the following (see, e.g., [24, 25, 26, 27]) relativistic fluid equations coupled to the electromagnetic field via:

$$\partial_\mu T_{(s)}^{\mu\nu} = F^{\nu\alpha} j_{\alpha(s)}, \quad (2.2)$$

where

$$T_{(s)}^{\mu\nu} = h_s U_{(s)}^\mu U_{(s)}^\nu + p_s \eta^{\mu\nu} \quad (2.3)$$

and

$$F^{\mu\nu} = \partial^\mu A^\nu - \partial^\nu A^\mu \quad (2.4)$$

are, respectively, the energy-momentum tensor of the fluid species  $s$  and the electromagnetic field tensor. Greek indices run from 0 to 3. With the following

definitions:  $U_s^\mu = \{\gamma_s, \gamma_s \mathbf{V}_s/c\}$  is the fluid four-velocity,  $\gamma = (1 - V^2/c^2)^{-1/2}$  is the Lorentz factor,  $A^\mu = \{\phi, \mathbf{A}\}$  is the four vector potential,  $\eta^{\mu\nu} = (-1, 1, 1, 1)$  is the Minkowski tensor,  $j_{(s)}^\mu = q_s n_{R(s)} U_{(s)}^\mu$  is the four current,  $p_s$  is the pressure and  $h_s$  is the enthalpy density per unit volume given by [24]

$$h_s = n_R m_s c^2 \frac{K_3(z_s)}{K_2(z_s)} \equiv n_R m_s c^2 G(z_s), \quad (2.5)$$

where  $K_j$  is the modified Bessel function of  $j$  kind, with argument  $z_s = m_s c^2 / T_s$ ;  $q_s$ ,  $m_s$ ,  $n_R$  and  $T_s$  are respectively the invariants: charge, rest mass, rest density and temperature for the species  $s$ . The relativistic equations of motion (2.2) can be broken down into their zero and three components. The three or vector component gives (the zero component would not be used):

$$n_s \frac{d}{dt} (m_s G_s \gamma_s \mathbf{V}_s) + \nabla p_s = q_s n_s [\mathbf{E} + (\mathbf{V}_s \times \mathbf{B})/c] \quad (2.6)$$

where  $d/dt \equiv \partial/\partial t + \mathbf{V}_s \cdot \nabla$ . Equation (2.6) shows that when temperature effects are properly included the effective momentum of the charged fluid  $s$ , becomes  $\mathbf{P} = mG\gamma\mathbf{V}$ . Note that  $G(z_s)$  is a function of temperature only. To proceed, we assume that our system is a two-fluid system. That is, the system is composed of two types of particles. The particles' masses could greatly differ (or be equal) but their charges are equal and opposite, namely: positive (+) and negative (-). Then the equation of motion (2.6) can be cast in a vortex dynamical form by taking its curl<sup>1</sup>

$$\frac{\partial \mathbf{\Omega}_\pm}{\partial t} = \nabla \times (\mathbf{V}_\pm \times \mathbf{\Omega}_\pm), \quad (2.7)$$

---

<sup>1</sup>The term  $\nabla \times (n^{-1} \nabla p) \neq 0$  even for barotropic pressure, that is  $p = p(n)$ , because of the  $\gamma$  factor that is a function of space and time ( $n = \gamma n_R$ ). However one can write it out as  $\nabla \times (n^{-1} \nabla p) \propto \nabla T \times \nabla \sigma = 0$  for homogeneous entropy  $\sigma$ . Where  $\nabla h = T \nabla \sigma + n^{-1} \nabla p$ .

where

$$\boldsymbol{\Omega}_{\pm} \equiv \mathbf{B} \pm \mu_{\pm} \nabla \times \gamma_{\pm} \mathbf{V}_{\pm} \quad (2.8)$$

is the generalized vorticity. Here, velocities have already been normalized to the speed of light  $c$ , lengths to  $c/\bar{\omega}_c$ , time to  $\bar{\omega}_c$  and magnetic field to a uniform ambient field  $B_o$ . With the following definitions:  $\gamma_{\pm} = (1 - |\mathbf{V}_{\pm}|^2)^{-1/2}$ ,  $\mu_{\pm} \equiv \bar{m}_{\pm}/(\bar{m}_+ + \bar{m}_-)$ ,  $\bar{\omega}_c = eB_o/c(\bar{m}_+ + \bar{m}_-)$ ,  $\bar{\omega}_p^2 = 4\pi n_o e^2/(\bar{m}_+ + \bar{m}_-)$ ,  $n_+ = n_- \equiv n_o$ ; where  $e$  is the electron's charge magnitude and  $n_o$  is the uniform density in each fluid's rest frame.

Notice that  $\mu$  is a reduced mass and  $\bar{m}_{\pm} = m_o G(z_{\pm})$  should be viewed as an “effective mass” that depends on the temperature through the function  $G(z_{\pm}) = K_3(z_{\pm})/K_2(z_{\pm})$  with argument  $z_{\pm} = m_o/T_{\pm}$ ;  $m_o$  represents the rest (bare) mass for each species. For example, for ion-electron plasmas it is different for each species.

- For low temperatures  $T_{\pm} \ll m_o$ , the large argument expansion ( $z_{\pm} \gg 1$ ) of  $G(z_{\pm})$  gives  $G(z_{\pm}) \approx 1 + (5/2)T_{\pm}/m_o$ , therefore

$$\bar{m}_{\pm} \approx m_o + \frac{5}{2}T_{\pm}. \quad (2.9)$$

Thus, the effective mass is composed of the rest (bare) mass and a small temperature contribution. By using this limit in Eq. (2.5), one immediately recognizes the familiar expression for the enthalpy of a perfect non-quantum gas of point particles. That is,

$$h_{\pm} = n_o m_o c^2 + \frac{5}{2} n_o T_{\pm}. \quad (2.10)$$

In a cold plasma, of course,  $\bar{m}_\pm = m_o$ .

- For ultra-relativistic temperatures  $T_\pm \gg m_o$  ( $z_\pm \ll 1$ ), then  $G(z_\pm) \approx 4T_\pm/m_o$ , leading to

$$\bar{m}_\pm \approx 4T_\pm. \quad (2.11)$$

Equation (2.7) represents a system of two equations with three unknowns. The system is completed by using the curl of Ampere's Law, which in our normalizations becomes:

$$\nabla \times (\nabla \times \mathbf{B}) + \frac{\partial^2 \mathbf{B}}{\partial t^2} = \frac{c^2}{\bar{V}_A^2} \nabla \times [\gamma_+ \mathbf{V}_+ - \gamma_- \mathbf{V}_-], \quad (2.12)$$

where  $\bar{V}_A = B_o/\sqrt{4\pi n_o(\bar{m}_+ + \bar{m}_-)}$ . Note that in Eq. (2.12) the explicit expression for the current,  $\mathbf{j} = en_o(\gamma_+ \mathbf{V}_+ - \gamma_- \mathbf{V}_-)$ , has been used; which makes it valid in any frame. From now on, we assume that the equilibrium species temperatures are equal ( $T_+ = T_- = T$ ) and we call  $G(z)$  simply  $G(T)$ .

It is important to mention that this fluid model, composed of equations (2.7) and (2.12), is fully relativistic, both in directed speed as well as in temperature. One can see from Eq. (2.11), for example, that for high relativistic temperatures, the fluid's inertia is no longer provided by the mass, but rather by the random motion of the particles. This is the model we will use to study relativistic waves in astrophysical plasmas. But before that, we need to introduce the physics of pulsar magnetospheres.

## Chapter 3

# Physics of Pulsars Magnetospheres

### 3.1 Introduction

The pulsar's radio emissions are thought to be generated in a region called the pulsar magnetosphere. The magnetosphere is, as one can infer from its name, a magnetized atmosphere, but unlike the Earth's, it is charged. The basic description of the magnetosphere due to Goldreich and Julian (1969, hereafter GJ) [28] is known to be incomplete. One of the reasons is that their model assumes that the magnetic and rotational axes are aligned, and therefore such a model cannot account for the lighthouse effect. Nevertheless, it was the first model to point out that pulsars have magnetospheres and it forms the basis for almost all theoretical studies of pulsars magnetospheres. The energetics of the emission region were pioneered by Sturrock (1971) [29] and Ruderman and Sutherland (1975) [30] (hereafter SRS). The SRS energetic (emission) models, which are based on the GJ model, were the first to give a detailed explanation of the characteristics and properties of the pulsar polar caps. For this reason, the combined model of GJ and SRS, is called the "Pulsar Standard Model."

In this chapter we will describe the most important aspects of this

model. We will first show that, if the neutron star is considered as a conducting magnetized sphere, then, due to induced electric fields, it cannot be surrounded by vacuum. Assuming, then, that the star has an atmosphere, its electrostatics will be described.

### 3.2 Pulsar magnetosphere: standard model

Because neutron stars have strong gravitational fields at their surfaces, usually  $10^8$  times larger than the Earth's, the first studies of the pulsar magnetosphere assumed essentially vacuum conditions (see, for example, Pacini (1967) [16], Gold (1968) [17]). However Goldreich and Julian (1969) showed that this is not the case. Knowing that the conductivity of a neutron star is extremely high (see, for example, Manchester and Taylor [23]) and can be considered infinite, they argued that inside the star  $\mathbf{E} \cdot \mathbf{B} = 0$ , or

$$[\mathbf{E} + (\mathbf{w} \times \mathbf{r}) \times \mathbf{B}/c]_{in} = 0, \quad (3.1)$$

where  $w = 2\pi/P$  is the angular velocity of the star ( $P$  is the period), and  $\mathbf{E}$  and  $\mathbf{B}$  are the electric and magnetic fields. A neutron star in vacuum, idealized as a magnetized conducting sphere with (dipole) magnetic and rotation axes parallel, the Laplace's equation, together with boundary conditions at the surface, gives a quadrupolar potential

$$\phi(r, \theta) = -\frac{wB_oR^5}{6r^3c}(3\cos^2\theta - 1), \quad (3.2)$$

where  $\theta$  is the angle from the rotation axis,  $R$  is the star's radius and  $B_o$  is the magnetic field strength at the surface. What Goldreich and Julian realized is,

that the electric field, associated with the quadrupolar potential given in Eq. (3.2), has a nonzero component along the magnetic field at the surface of the star

$$(\mathbf{E} \cdot \mathbf{B})_{r=R} = -\frac{wRB_o^2}{c} \cos^3 \theta \neq 0. \quad (3.3)$$

Thus for a pulsar with period  $P = 0.2$  s and  $B_o = 10^{12}$  G the corresponding parallel electric field strength is

$$E_{\parallel} \approx \frac{wB_oR}{c} \approx 10^9 \text{ V cm}^{-1}. \quad (3.4)$$

This exerts on an electron an enormous force ( $q = 5 \times 10^{-10}$  statCoul)

$$F_e = qE_{\parallel} \approx 5 \times 10^{-1} \text{ dynes}, \quad (3.5)$$

which is 12 orders of magnitude larger than the star's gravitational force ( $M = 1.5M_s$ )

$$F_g \approx 2 \times 10^{-13} \text{ dynes}. \quad (3.6)$$

Hence charge particles (electrons mainly) at the star's surface will be ejected into its surroundings, undermining the vacuum assumption and forming the magnetosphere. The energy for ripping particles off the star's surface comes from the electric field Eq. (3.3) induced by the rotation of the magnetized star. Since the energy is of rotational origin with time the pulsar's rotational speed must slow down, as stated in the introduction.

Since strong induced electric fields pull material to fill the star's surroundings. Suppose now that there is an ample supply of plasma (surrounding

the star) such that

$$\mathbf{E} + \mathbf{V} \times \mathbf{B}/c = 0. \quad (3.7)$$

Since Eq. (3.7) implies that the plasma is “frozen” to the magnetic field lines and these are anchored to the star, then the velocity of the plasma can be taken to be  $\mathbf{V} = \boldsymbol{\omega} \times \mathbf{r}$ . Thus the whole magnetosphere corotates as a solid body with the star. However, as one moves away from the star (larger radius) the velocity increases, and corotation cannot be maintained beyond a surface, where  $V \sim c$ , called the light cylinder, with radius

$$R_L = c/\omega \approx 5 \times 10^9 \left( \frac{P}{s} \right) \text{ cm} \quad (3.8)$$

where  $P$  is in seconds. The associated charge density to Eq. (3.7) is given by

$$\rho = \frac{1}{4\pi} \nabla \cdot \mathbf{E}. \quad (3.9)$$

Using  $\mathbf{E} = -\mathbf{V} \times \mathbf{B}/c$ , a vector identity<sup>1</sup> and knowing that the vorticity (with spherical symmetry) is  $\nabla \times \mathbf{V} = 2\boldsymbol{\omega}$ , we get

$$\rho = -2\mathbf{B} \cdot \boldsymbol{\omega}/c + \mathbf{V} \cdot \nabla \times \mathbf{B}/c. \quad (3.10)$$

After using Ampere’s law on Eq. (3.10) (second term right hand side) we finally obtain

$$\rho_{GJ} = -\frac{\boldsymbol{\omega} \cdot \mathbf{B}}{2\pi c} \left[ 1 - \frac{V^2}{c^2} \right]^{-1} \equiv -\frac{\boldsymbol{\omega} \cdot \mathbf{B}}{2\pi c} f \quad (3.11)$$

where  $f = 1 + O(V^2/c^2) = 1 + O(\omega^2 r^2/c^2)$ . Equation (3.11) is called the Goldreich-Julian or “corotating” density. It is the minimum density necessary

---

<sup>1</sup> $\nabla \cdot (\mathbf{A} \times \mathbf{B}) = \mathbf{B} \cdot \nabla \times \mathbf{A} - \mathbf{A} \cdot \nabla \times \mathbf{B}$

to screen out the parallel electric field ( $\vec{E} \cdot \vec{B} = 0$ ) in the magnetosphere. The  $f$  factor emphasizes that the corotating density is only valid inside the light cylinder; see Fig. 3.1.

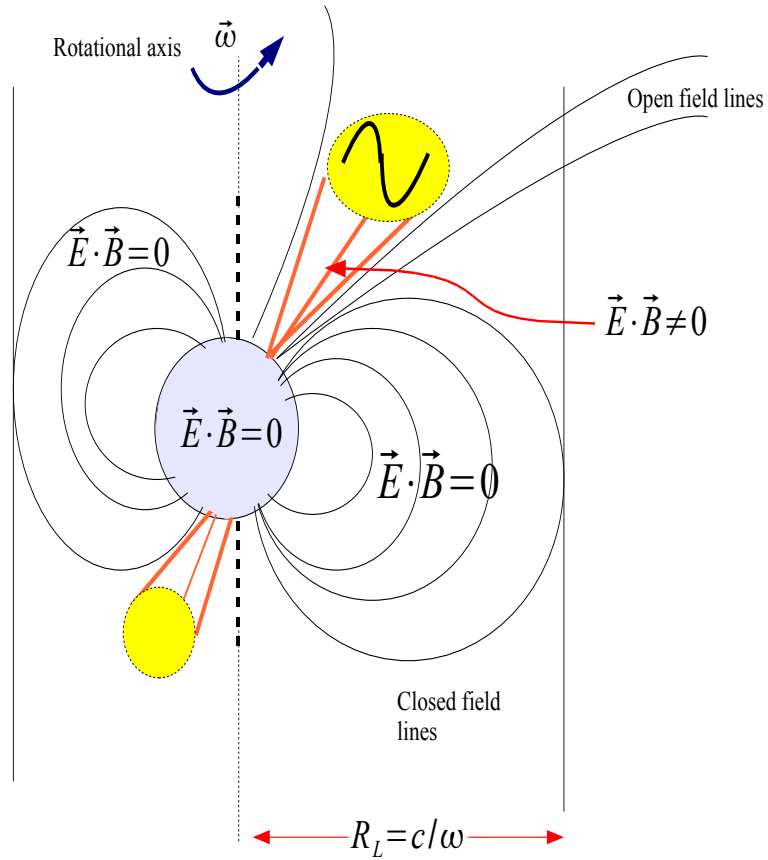


Figure 3.1: Pulsar magnetosphere.

On Fig. 3.1 two distinct regions are shown, the closed field lines that do not penetrate the light cylinder and the open field lines that leave the star

and penetrate the light cylinder. The open field line region defines the polar cap which is centered on the star's magnetic pole.

### 3.2.1 Polar cap model

The neutron star's polar cap is defined by the “last open field line”. However, in order to make numerical estimates of its size, we will use the “last closed field line”, that is, the magnetic field line tangential to the light cylinder surface. The equation for a (dipole) magnetic field line (in polar coordinates) is

$$r = r_o \sin^2 \theta, \quad (3.12)$$

for the last closed field line we have that  $r_o = R_L$ . Furthermore, as we can see on Fig. 3.2,  $\theta_p$  is the angle, from the magnetic axis to the last closed magnetic field line. At this angle ( $r = R$ )

$$R = R_L \sin^2 \theta_p, \quad (3.13)$$

or

$$\sin \theta_p = \sqrt{\frac{2\pi R}{cP}} \quad (3.14)$$

where we have used  $R_L = c/w$ . Therefore we can estimate the size of the polar cap radius

$$R_p \simeq R \sin \theta_p = \sqrt{\frac{R^3 2\pi}{cP}} \approx 1.5 \times 10^4 \text{ cm} \left(\frac{s}{P}\right)^{1/2} \quad (3.15)$$

for  $R = 10 \text{ km} = 10^6 \text{ cm}$ . With magnetic and rotational axes parallel, the potential, at the center of the pole, will be negative with respect to the stellar

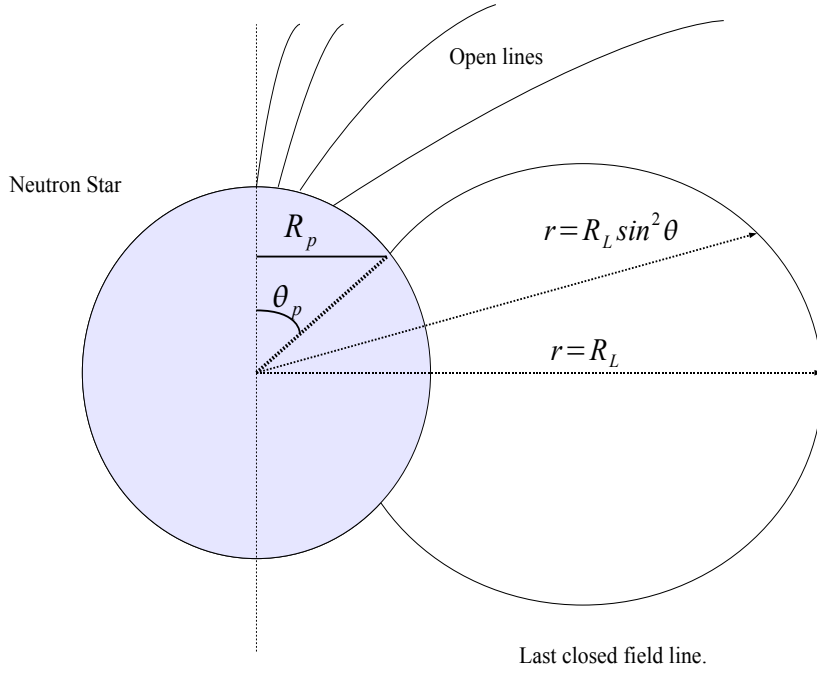


Figure 3.2: Polar Cap Region.

environment, therefore electrons will stream along these lines from the star (or equivalently one can find the electric field [Eq. (3.3)], at the center of the pole, to be negative). The potential drop from the center of the pole to the edge of the polar cap, can be estimated, from Eqs. (3.2) and (3.15), to be

$$\Delta\phi \approx \frac{1}{2}RB_o \left( \frac{wR}{c} \right)^2 \sim 10^{11} - 10^{12} \text{ V.} \quad (3.16)$$

Consequently, particles with energies

$$\mathcal{E} = q\Delta\phi \sim 10^{12} - 10^{14} \text{ eV} \quad (3.17)$$

are expected. The Lorentz factor associated with these energies is

$$\gamma = \frac{\mathcal{E}}{m_e c^2} \sim 10^7, \quad (3.18)$$

these particles constitute the primary particles in the SRS model [30].

### 3.2.2 Pair ( $e^-$ , $e^+$ ) plasmas

According to the SRS model, the high energetic charged primary particles will move along the open magnetic field lines. Their distribution becomes one dimensional in momentum space, after they loose their perpendicular momentum through synchrotron radiation. The synchrotron radiation energizes the stellar environment (nebula) surrounding the pulsar. As the primary particles keep streaming along  $B$ , they emit curvature radiation photons since the magnetic lines are curved. The frequency of the “curvature photons” is

$$\omega_{cur} \approx \gamma^3 \frac{c}{r_c} \sim 10^{23} \text{ s}^{-1}, \quad (3.19)$$

that is, the radiation would be in  $\gamma$ -rays;  $r_c = 10^8$  cm is the radius of curvature and  $\gamma = 10^7$ . The curvature photons, constrained to move along field lines, will eventually (since lines are curved) interact with the magnetic field producing pairs  $\gamma + B \rightarrow e^- + e^+$ , see Fig. 3.3. These pairs are so energetic that they may radiate and go on to produce further pairs, creating an avalanche of secondary particles. The secondary particles may be born into an excited Landau level with energies  $E^2/m^2 c^4 = 1 + p_{\parallel}^2/m^2 c^2 + (2n + 1 \pm s)B/B_{cr}$  where  $p_{\parallel}$  is the momentum along  $B$ ;  $B_{cr} = m^2 c^3 / e \hbar \sim 4.4 \times 10^{13}$  G is the critical magnetic field, the spin  $s$  can be  $\pm 1$  and  $n$  is a nonnegative integer specifying

the Landau level [7, 31]. After rapid synchrotron emission, the newly created pairs that emit in these strong fields will be in the ground state,  $n = 0$  and  $1 \pm s = 0$ , constrained to move along  $\mathbf{B}$ . The “gap” ( $\mathbf{E} \cdot \mathbf{B} \neq 0$ ) or the

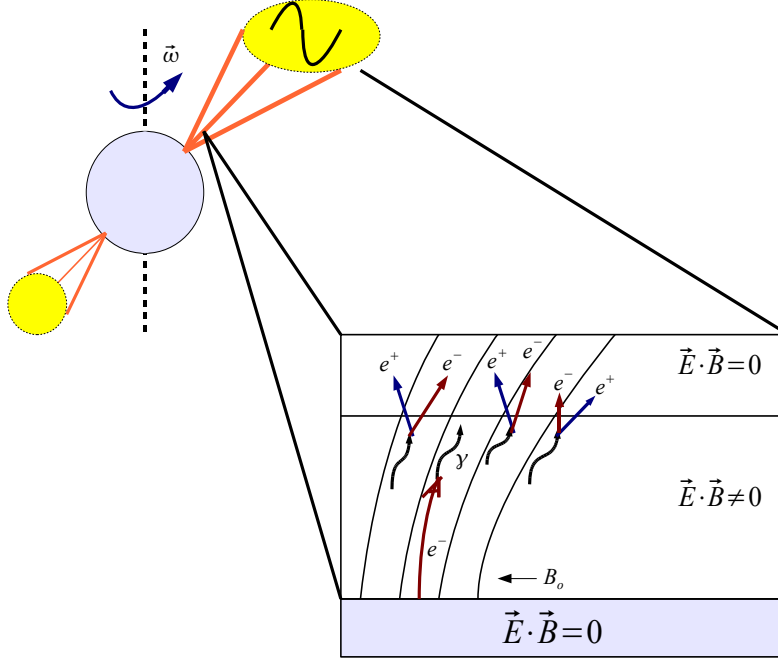


Figure 3.3: Pair production at the poles of neutron stars.

region where the above processes occur will eventually stop growing, after the population of secondary pairs increases dramatically, such that, the condition  $\mathbf{E} \cdot \mathbf{B} = 0$  is achieved. It is in this region (where there is an ample supply of pair plasma) that the observed radio emissions are produced. According to the SRS model, the density of the pair plasma is  $n_{\pm} = \Gamma n_{GJ}$ , where  $\Gamma \sim 10^3 - 10^6$  is a multiplication factor,  $n_{GJ} = -\boldsymbol{\omega} \cdot \mathbf{B} / 2\pi ec \approx 10^{11} \text{ cm}^{-3}$  is the “corotating” or GJ density. The energy of the pair plasma is  $\gamma_{\pm} = (n_b / n_{\pm}) \gamma_b \approx 10^3$ , where

$n_b \sim n_{GJ}$  and  $\gamma_b \sim 10^7$  are, respectively, the density and Lorentz factor of the primary beam.

Another property of the pair plasma is the relative streaming between components. The possibility of streaming of this secondary plasma comes from the requirement that the total charge density of the three components (primary beam plus electrons and positrons) must be equal to the corotating charge density, that is

$$\rho_b + \rho_+ + \rho_- = \rho_{GJ}, \quad (3.20)$$

such that the parallel electric field is zero ( $\mathbf{E} \cdot \mathbf{B} = 0$ ). Now, in the absence of further pair creation or recombination, the three currents must be conserved (constants), that is,  $\nabla \cdot \mathbf{j}_i = 0$ , where  $i = 1, 2, 3$ . Therefore, for the primary beam  $\nabla \cdot \mathbf{j}_b = 0$  implying  $j_b = en_b c = \kappa B$ , where  $\kappa = \text{constant}$ . From this we obtain that  $n_b \propto B$ . For the secondary plasma components  $j_{\pm} = \rho_{\pm} v_{\pm} = \pm j_p = \text{const}$ . Since the pair plasma is neutral, then at the discharge region (pair formation front) Eq. (3.20) implies

$$\rho_b = \rho_{GJ}, \quad (3.21)$$

thus, the initial charge density must be supplied by the primary charged beam. The situation changes as the flow propagates along  $B$ , because  $n_{GJ} \propto B \cos \theta$  ( $\theta$  is the angle between  $w$  and  $B$ ), while  $n_b \propto B$ . Thus a deviation develops between the two. Consequently, one type of secondary particles will be accelerated (say, electrons) and the other (positrons) will be decelerated, such

that

$$\rho_b + j_p \left( \frac{1}{v_+} - \frac{1}{v_-} \right) = \rho_{GJ} \quad (3.22)$$

holds at every point, screening out the electric field that could result from that deviation. In the comoving center of momentum (CM) frame, i.e., the frame that moves with the speed at which the pair was created, the positive and negative streams move in opposite directions [32]. Therefore a streaming (also called counter-streaming) effect will be produced.

Another important property is their temperature and, more importantly, their distribution function. The distribution function is critical in determining the exact properties of waves in  $e^-$ ,  $e^+$  plasmas. Many of the existing calculations in the literature have assumed analytically convenient distribution functions without physical justification. However, recently, Arendt and Eilek (2002) [7] have demonstrated that the distribution function of these plasmas is very likely Maxwellian with temperatures very close to  $T \sim m_o c^2$ . Therefore, it is very important to determine the exact properties of waves in these plasmas at such temperatures. For this, we investigate the relativistic fluid model introduced in Chapter 2 to study propagation of waves in streaming magnetized pair plasmas.

## Chapter 4

# Relativistic Waves in Pulsar Plasmas

### 4.1 Introduction

We begin our study of relativistic waves in pulsar plasmas. Such plasmas, as we mentioned above, are composed of the secondary relativistic electron-positron ( $e^-e^+$ ) beams that stream along the magnetic field lines coming from the poles of neutron stars. In such a scenario, we study relativistic linear waves using the relativistic fluid model introduced in Chapter 2.

First, we give a brief introduction to the analysis of linear waves in plasmas. Then, we proceed to study waves at three angles of propagation: parallel, perpendicular and oblique. For parallel propagation we find four modes. One of them is unstable at short  $k$ . We analyze the implications of relativistic temperatures in all the modes found. We find the slow Alfvén mode to be two-stream unstable at long wave lengths and we show that this instability is not suppressed at temperatures of  $T \sim mc^2$ . We also analyze dispersion relations in the non-streaming limit.

We also calculate dispersion relations in a super strong magnetic field and show that as temperature increases the cutoffs decreases. Last, we give

numerical estimates of the growth rate (unstable mode) using the pulsar’s constraints, and comment on the results and their implications for theories of radio wave emissions. In this chapter we will follow Ref. [33].

#### 4.1.1 Basic concepts

In the study of a dynamical system, linear analysis provides the simplest and non-trivial, self-consistent method for solving any set of partial differential equations that describes the physics or dynamics of a system. If, for example,  $\chi(\mathbf{x}, t)$  and  $\zeta(\mathbf{x}, t)$  represent the dependent variables, that describes physical quantities in the dynamical system, and if the system allows a physical perturbation, such as  $\epsilon\chi_1$ , where  $\epsilon \ll 1$  is a small quantity, then

$$\chi = \chi_o + \epsilon\chi_1, \tag{4.1}$$

here  $\chi_o$  is the “zero order” or equilibrium variable and  $\epsilon|\chi_1| \ll |\chi_o|$  for all  $\mathbf{x}$  and  $t$ . The system of differential equations makes the other variables dependent on  $\chi$ , for example,

$$\zeta = \zeta(\chi) = \zeta(\chi_o + \epsilon\chi_1). \tag{4.2}$$

Since the dependence of  $\zeta$  on  $\chi$  is not linear in general, Taylor expanding  $\zeta$  gives

$$\zeta = \zeta_o + \epsilon\zeta_1 + \epsilon^2\zeta_2 + \dots \tag{4.3}$$

The  $\epsilon$ 's will be, from now on, considered implicit and so the dependent variables are written as

$$\chi = \chi_o + \chi_1 \tag{4.4}$$

$$\zeta = \zeta_o + \zeta_1 + \zeta_2 + \dots \tag{4.5}$$

The essence of linearization consists, after substitution of the dependent variables' expansions in the differential equations, in keeping terms of order one only, that is, eliminating terms of higher order such as  $\zeta_2$ , and products  $\chi_1\zeta_1$ , etc. What remains are linearized differential equations.

One method for solving the now linearized equations is by assuming that all the perturbed quantities (dependent variables) are of the form  $\sim \exp(i\mathbf{k} \cdot \mathbf{x} - i\omega t)$ , that is, plane wave solutions.

In the study of linear waves in plasmas, one is interested on the relation between frequency  $\omega$  and wavelength  $k = 2\pi/\lambda$ . This relation is called *dispersion relation*. Among other things, the dispersion relation tells us at what speed waves propagate in a medium. For example, the dispersion relation for an electromagnetic wave in vacuum is  $\omega = kc$ . Therefore the velocity at which this wave propagates is given by  $v_g = d\omega/dk = c$ , that is, the speed of light. In a plasma, or any dispersive medium, the situation is usually not that simple since the speed will depend on the wavelength of the wave itself  $\omega = c(\lambda)k$ ; that is, different waves will travel at different speeds.

## 4.2 Linear waves in pulsars

We investigate linear waves in a region far from the surface of the neutron star, such that the magnetic field  $B$  is still strong, but less than the critical value  $B_{cr} = (m_e^2 c^3 / e \hbar) \approx 4.4 \times 10^{13}$  G, so that all quantum effects can be ignored. We also neglect the curvature of the pulsar magnetic field, this can be justified for wave lengths satisfying  $\lambda \ll B / (\partial B / \partial r)$ , that is, when the wavelength is much less than the scale length of the magnetic field inhomogeneity. Such a system could be studied in Cartesian coordinates. One, must make sure that the  $e^-$ - $e^+$  plasmas are sufficiently long lived for collective effects to be observed. It has been shown in Refs. [34, 35] that annihilation rates for electron-positrons (or positronium bound state formations) are much longer than the characteristic scale times for collective oscillations, typical plasma frequencies (at densities of interest), such that the pair plasma will live sufficiently long for many collective oscillations to take place. Dissipation effects induced by Coulomb collisions can also be neglected due to the smallness of the  $e^-$ - $e^+$  (or  $e^-$ - $e^-$ ) scattering cross section  $\sigma \sim (e^2/E)^2 \sim 10^{-30} \text{cm}^2$  (at relativistic energies in the range  $\gamma \sim 10 - 10^2$ ). It should be pointed out different terminologies used in the literature to describe waves in e-p plasmas can create confusion see, e.g., [36]. Here we will use the conventional language used to describe the electron-ion plasmas.

To proceed we'll use the index  $\alpha$  to represent the particle species, which in our case takes only two values: positive or negative. Using a standard vector

identity <sup>1</sup> we can write Eq. (2.7) as

$$\partial_t \boldsymbol{\Omega}_\alpha = -\boldsymbol{\Omega}_\alpha (\nabla \cdot \mathbf{V}_\alpha) + (\boldsymbol{\Omega}_\alpha \cdot \nabla) \mathbf{V}_\alpha - (\mathbf{V}_\alpha \cdot \nabla) \boldsymbol{\Omega}_\alpha. \quad (4.6)$$

( $\nabla \cdot \boldsymbol{\Omega}_\alpha = 0$ ). We take, the equilibrium magnetic field

$$\mathbf{B} = B_o \hat{\mathbf{z}},$$

along the  $\hat{\mathbf{z}}$  axis and the equilibrium fluid velocities in the CM frame (the frame at which the pair was born), or equivalently in a frame in which they are equal, to be

$$\mathbf{V}_+ = -\mathbf{V}_o, \quad \mathbf{V}_- = \mathbf{V}_o,$$

where ( $V_o = \text{constant}$ )

$$\mathbf{V}_o = V_o \hat{\mathbf{z}}.$$

Thus electrons (positrons) move with positive (negative) velocity along  $\hat{\mathbf{z}}$ . To study linear waves, we expand

$$\mathbf{V}_\alpha = -\alpha \mathbf{V}_o + \mathbf{v}_\alpha, \quad (4.7)$$

$$\mathbf{B} = \hat{\mathbf{z}} + \mathbf{b} \quad (4.8)$$

where  $\mathbf{v}_\alpha$  and  $\mathbf{b}$  are the fluctuating quantities and  $\hat{\mathbf{z}}$  is a normalized (to  $B_o$ ) equilibrium field. Although we are linearly expanding  $\mathbf{V}_\alpha$ , we faced the problem of the inherent nonlinearity introduced by the  $\gamma_\alpha$  factor. However, we can

---

<sup>1</sup> $\nabla \times (\mathbf{A} \times \mathbf{B}) = \mathbf{A}(\nabla \cdot \mathbf{B}) - \mathbf{B}(\nabla \cdot \mathbf{A}) + (\mathbf{B} \cdot \nabla) \mathbf{A} - (\mathbf{A} \cdot \nabla) \mathbf{B}$

expand it as follows

$$\gamma_\alpha = (1 - \mathbf{V}_\alpha^2)^{-1/2} = [1 - (-\alpha \mathbf{V}_o + \mathbf{v}_\alpha)^2]^{-1/2} \quad (4.9a)$$

$$= (1 - V_o^2)^{-1/2} \left[ 1 + 2\alpha \frac{\mathbf{V}_o \cdot \mathbf{v}_\alpha}{(1 - V_o^2)} + O(v_\alpha^2) \right]^{-1/2}, \quad (4.9b)$$

which for sufficiently small  $\mathbf{v}_\alpha$ , Eq. (4.9b) gives

$$\gamma_\alpha \simeq \gamma_o - \alpha \gamma_o^3 \mathbf{V}_o \cdot \mathbf{v}_\alpha \quad (4.10)$$

where  $\gamma_o = (1 - V_o^2)^{-1/2} = \text{constant}$ . Using Eqs. (4.7), (4.8) and (4.10) in Eq. (2.8) we find

$$\boldsymbol{\Omega}_\alpha = \hat{\mathbf{z}} + \boldsymbol{\Omega}'_\alpha \quad (4.11)$$

where

$$\boldsymbol{\Omega}'_\alpha = \mathbf{b} + \frac{\alpha}{2} \nabla \times [\gamma_o \mathbf{v}_\alpha + \gamma_o^3 (\mathbf{V}_o \cdot \mathbf{v}_\alpha) \mathbf{V}_o] \quad (4.12)$$

is the perturbed vorticity. Then using Eqs. (4.7) and (4.12) and  $\nabla \cdot \mathbf{v}_\alpha = 0$ , we can linearize Eq. (4.6) to get

$$(\partial_t - \alpha \mathbf{V}_o \cdot \nabla) \boldsymbol{\Omega}'_\alpha = (\hat{\mathbf{z}} \cdot \nabla) \mathbf{v}_\alpha. \quad (4.13)$$

The system is closed with (2.12) which, after linearization, becomes

$$-\nabla^2 \mathbf{b} + \partial_t^2 \mathbf{b} = \frac{1}{d^2} \sum_\alpha \alpha \nabla \times [\gamma_o \mathbf{v}_\alpha + \gamma_o^3 (\mathbf{V}_o \cdot \mathbf{v}_\alpha) \mathbf{V}_o], \quad (4.14)$$

where  $d \equiv \bar{V}_A/c = \bar{\omega}_c/\bar{\omega}_p = \omega_c/[\sqrt{G}\omega_p]$ .

We solve the system of linearized equations by assuming that the fluctuating quantities,  $\mathbf{b}$ ,  $\mathbf{v}_\alpha$  vary like  $e^{i(\mathbf{k}\cdot\mathbf{r}-\omega t)}$ . We use Cartesian coordinates

with the  $\hat{z}$  axis along the ambient magnetic field and the wave vector  $\mathbf{k} = k(\sin \theta, 0, \cos \theta)$  in the  $\hat{x}$ - $\hat{z}$  plane. We also drop the primes from the perturbed vorticities to simplify the notation. With these assumptions Eqs. (4.13) and (4.14) become

$$(\omega + \alpha V_o k \cos \theta) \Omega_x^\alpha = -k \cos \theta v_x^\alpha \quad (4.15a)$$

$$(\omega + \alpha V_o k \cos \theta) \Omega_y^\alpha = -k \cos \theta v_y^\alpha \quad (4.15b)$$

$$(\omega + \alpha V_o k \cos \theta) \Omega_z^\alpha = -k \cos \theta v_z^\alpha, \quad (4.15c)$$

$$(k^2 - \omega^2) b_x = \frac{1}{d^2} [-i \gamma_o k \cos \theta (v_y^+ - v_y^-)] \quad (4.16a)$$

$$(k^2 - \omega^2) b_y = \frac{1}{d^2} [i \gamma_o k \cos \theta (v_x^+ - v_x^-) - i \gamma_o^3 k \sin \theta (v_z^+ - v_z^-)] \quad (4.16b)$$

$$(k^2 - \omega^2) b_z = \frac{1}{d^2} [i \gamma_o k \sin \theta (v_y^+ - v_y^-)], \quad (4.16c)$$

where

$$\Omega_x^\alpha = b_x + \frac{\alpha}{2} [-i \gamma_o k \cos \theta v_y^\alpha] \quad (4.17)$$

$$\Omega_y^\alpha = b_y + \frac{\alpha}{2} [i \gamma_o k \cos \theta v_x^\alpha - i \gamma_o^3 k \sin \theta v_z^\alpha] \quad (4.18)$$

$$\Omega_z^\alpha = b_z + \frac{\alpha}{2} [i \gamma_o k \sin \theta v_y^\alpha]. \quad (4.19)$$

The system of Eqs. (4.15)-(4.16) consists of 9 equations and 9 unknowns. However, they are not independent since we have used  $\nabla \cdot \mathbf{v} = 0$  (together with  $\nabla \cdot \mathbf{b} = 0$ ). In fact it's not difficult to see that the set of equations

(4.15a), (4.15b) and (4.16a), (4.16b) represent all the independent equations.

This set is reducible to the matrix

$$\begin{pmatrix} \frac{1}{\omega_D^\pm} & 0 & -i\gamma_o P & i\frac{\gamma_o}{L} \\ 0 & \frac{1}{\omega_D^\pm} & -i\frac{\gamma_o}{L} & i\gamma_o P \\ i\gamma_o[\cos^2\theta + \gamma_o^2 \sin^2\theta]P & -i\frac{\gamma_o}{L}[\cos^2\theta + \gamma_o^2 \sin^2\theta] & \frac{\cos^2\theta}{\omega_D^\pm} & 0 \\ i\frac{\gamma_o}{L}[\cos^2\theta + \gamma_o^2 \sin^2\theta] & -i\gamma_o[\cos^2\theta + \gamma_o^2 \sin^2\theta]P & 0 & \frac{\cos^2\theta}{\omega_D^\pm} \end{pmatrix} \begin{pmatrix} v_x^+ \\ v_x^- \\ v_y^+ \\ v_y^- \end{pmatrix} = 0 \quad (4.20)$$

where we have used the following abbreviations to simplify the notation:  $L \equiv d^2(k^2 - \omega^2)$ ,  $P \equiv 1/L + 1/2$ ,  $\omega_D^\pm \equiv \omega \pm V_o k \cos\theta$ .

#### 4.2.1 Waves propagating parallel ( $\mathbf{k} \parallel \hat{\mathbf{z}}$ )

When wave propagation is along the magnetic field ( $\theta = 0$ ), the determinant of Eq. (4.20) gives the dispersion relation

$$0 = 1 + \frac{2\gamma_o^2}{L^2}(\omega^2 - k^2 V_o^2) - 2\gamma_o^2(\omega^2 + k^2 V_o^2) \left(\frac{1}{2} + \frac{1}{L}\right)^2 + \gamma_o^4(\omega - kV_o)^2(\omega + kV_o)^2 \left[\left(\frac{1}{2} + \frac{1}{L}\right)^2 - \frac{1}{L^2}\right]^2. \quad (4.21)$$

Equation (4.21) gives us four transverse modes. The frequencies of the first two transverse modes are

$$\omega_{(1)} = \left[ \frac{2}{d^2} + \frac{2}{\gamma_o^2} \mp \frac{2V_o k}{\gamma_o} + (1 + V_o^2) \frac{k^2}{2} + \frac{1}{2\gamma_o^2 d^2} \left\{ [4\gamma_o^2 + 4d^2 \mp 4\gamma_o V_o d^2 k + \gamma_o^2 d^2 (1 + V_o^2) k^2]^2 - 4\gamma_o^2 d^2 \Upsilon_\mp \right\}^{1/2} \right]^{1/2}. \quad (4.22)$$

Where

$$\Upsilon_{\mp} = \mp 8\gamma_o V_o k + 4(\gamma_o^2 V_o^2 + d^2)k^2 \mp 4\gamma_o V_o d^2 k^3 + \gamma_o^2 V_o^2 d^2 k^4.$$

These frequencies are electromagnetic plasma (EMP) modes (see Fig. 4.1), becoming asymptotic to  $kc$  at large  $k$ . Both modes are superluminal ( $V_\phi = \omega/k > c$ ); however solution one, corresponding to the upper signs, is slower than solution two. Both modes have cutoff ( $k \rightarrow 0$  limit) at

$$\omega^2 = \frac{4}{d^2} + \frac{4}{\gamma_o^2} = \frac{4\bar{\omega}_p^2}{\bar{\omega}_c^2} + \frac{4}{\gamma_o^2} \quad (4.23)$$

or in physical units:

$$\omega^2 = 4\frac{\omega_p^2}{G(T)} + 4\frac{\omega_c^2}{\gamma_o^2 G(T)^2} \quad (4.24)$$

the hybrid frequency. We have made the temperature explicit in (4.24). Note that  $\bar{\omega}_p^2 = \omega_p^2/G$  where  $\omega_p^2 = (4\pi n_o e^2/2m_o)$ ; likewise  $\bar{\omega}_c = \omega_c/G$  where  $\omega_c = (eB_o/c2m_o)$ . Equation (4.24) is our first important result. Note how the temperature affects the cutoff; for example, for ultra relativistic high temperatures ( $T \gg m_o$ ) the cutoff decreases. Since  $T \gg m_o$  implies  $G \approx 4T/m_o$ , then the effective mass becomes  $\bar{m} \approx 4T \gg m_o$ . Therefore the fluid inertia is primarily provided by the random thermal motion of the particles. If, on the other hand,  $T \ll m_o$ ,  $G(T) \approx 1$ , we recover the cold plasma cutoff [6]

$$\omega^2 = 4\omega_p^2 + 4\frac{\omega_c^2}{\gamma_o^2}. \quad (4.25)$$

In the large  $k$  limit, however, these EMP waves [Eqs. (4.22)] become

$$\begin{aligned} \omega &\approx \left[ \mp \frac{2V_o k}{\gamma_o} + (1 + V_o^2) \frac{k^2}{2} + \frac{k^2}{2}(1 - V_o^2) \pm \frac{2V_o k}{\gamma_o} \right]^{1/2} \\ &\approx k, \end{aligned} \quad (4.26)$$

the vacuum dispersion relation. In physical units Eq. (4.26) is

$$\frac{\omega}{\bar{\omega}_c} \approx k \frac{c}{\bar{\omega}_c} \Rightarrow \omega = kc. \quad (4.27)$$

Thus in this large  $k$  limit temperature effects are negligible. Therefore these modes are affected by temperature for long wavelengths only. As you go from cold to hot plasma the modes go from EMP to light waves; see Figs. 4.2 and 4.3. Particularly for secondary plasmas in pulsars  $T \sim m_o$  [ $G(1) \approx 4.37$ ] the two EMP modes are still present, see Fig. 4.2.

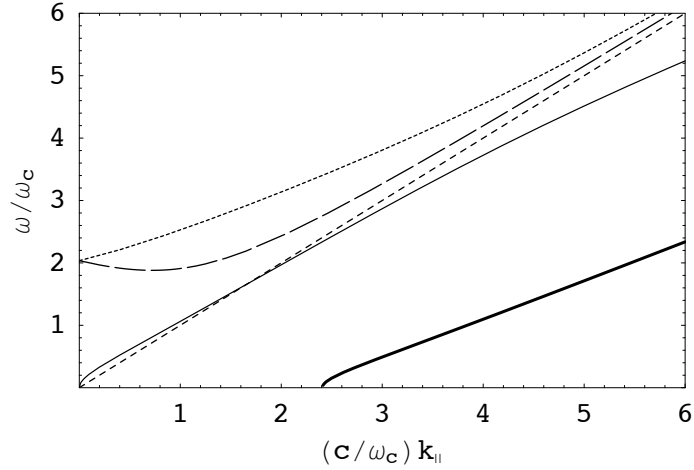


Figure 4.1: Dispersion curves for exactly parallel propagation ( $T \ll m_o$ ). There are four modes, the intermediate-dashed line is the vacuum dispersion  $\omega = kc$ . For the slow Alfvén mode (thick solid line)  $k < 2/V_o\gamma_o$  denotes the region of the cyclotron two-stream instability. The EMP modes (long and short dashed lines) have cutoff at  $\omega = \sqrt{4\omega_p^2/G + 4\omega_c^2/G^2\gamma_o^2}$ . The point  $k > 2\sqrt{\gamma_o^2 - 1}$  is where the fast Alfvén mode (continues line) becomes subluminal. The numerical parameters  $\gamma_o = 1.3$ ,  $d = 1.5$  where chosen for the sake of graphical clarity.

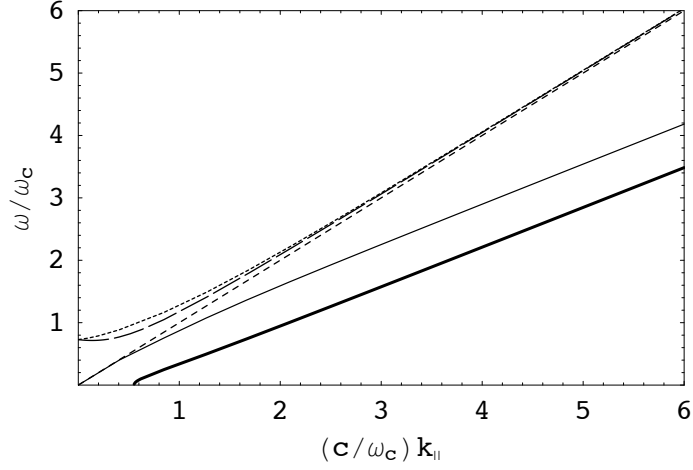


Figure 4.2: Dispersion curves for parallel propagation, for temperatures  $T = m_o$  ( $G = 4.37$ ). The labeling is the same used in Fig. 4.1. Note that, at short  $k$ , the degeneracy of the EMP modes is still present, and the slow Alfvén wave is still unstable.

The other two transverse modes are

$$\omega_{(4)}^{(3)} = \frac{1}{\sqrt{2}} \left[ \frac{4}{\gamma_o^2} + \frac{4}{d^2} \mp \frac{4V_o k}{\gamma_o} + k^2(1 + V_o^2) - \frac{1}{\gamma_o^2 d^2} \left\{ [4\gamma_o^2 + 4d^2 \mp 4\gamma_o V_o d^2 k + \gamma_o^2 d^2 (1 + V_o^2) k^2]^2 - 4\gamma_o^2 d^2 \Upsilon_{\mp} \right\}^{1/2} \right]^{1/2}. \quad (4.28)$$

Solution three, corresponding to the upper signs, will be called (see Sec. 4.2.1.2) the slow Alfvén wave; solution number four will be called the fast Alfvén wave (see Fig. 4.1). Of the two Alfvén waves, the fast mode is superluminal (for small wave vectors) becoming subluminal at  $kc > 2(\omega_c/G)\sqrt{\gamma_o^2 - 1}$ . The slow mode is always subluminal and is cyclotron two-stream unstable for small wave vectors. In fact there are two unstable regions

for this slow wave. The frequency vanishes at

$$k_{\pm} = \frac{1}{\gamma_o V_o G} \pm \frac{1}{\gamma_o V_o G} \left( 1 - 4 \frac{\gamma_o^2 V_o^2 G \omega_p^2}{\omega_c^2} \right)^{1/2} \quad (4.29)$$

and

$$k_c = \frac{2}{\gamma_o V_o}. \quad (4.30)$$

Thus the wave is unstable in the regions  $0 < k < k_-$  and  $k_+ < k < k_c$ , (see Fig. 4.4). If  $G \approx 1$  we recover the cold limit result for  $k_{\pm}$  [6]. Depending on the ratio  $(4\gamma_o^2 V_o^2 G \omega_p^2 / \omega_c^2)$ ,  $k_-$  and  $k_+$  can merge to form a sole region of instability  $0 < k < k_c$  (see Fig. 4.1).

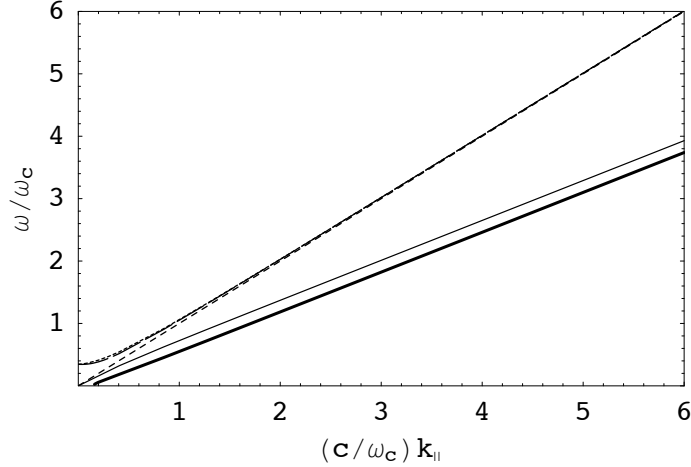


Figure 4.3: Dispersion curves for parallel propagation, for still higher temperatures  $T > m_o$ . The labeling is the same used in Fig. 4.1. Note that the EMP modes have virtually become light waves.

To understand better the critical wave vector  $k_c$  we find an approximate analytical expression by taking the small  $k$  limit of Eq. (4.28). After some

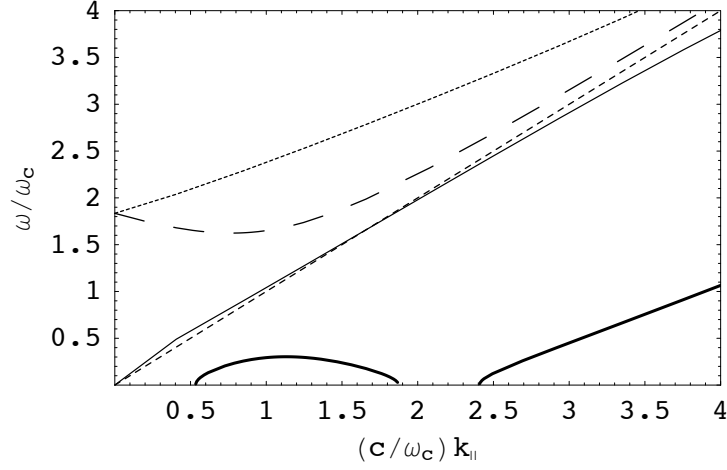


Figure 4.4: Dispersion curves for exactly parallel propagation with ratio  $4\gamma_o^2 V_o^2/d^2 < 1$ . Note that, as explained in text, the slow Alfvén wave (thick solid line) is unstable in two regions:  $0 < k < k_- \approx 0.53$  and  $k_+ \approx 1.87 < k < k_c \approx 2.41$ . The labeling for the rest of the curves is the same used in Fig. 4.1. The numerical parameters  $\gamma_o = 1.3$ ,  $d = 2$  where chosen for the sake of graphical clarity.

algebra we find

$$\omega_{(4)} \approx \sqrt{\frac{\mp 2V_o\gamma_o k + k^2(d^2/\gamma_o^2 + \gamma_o^2 V_o^2)}{\gamma_o^2 + d^2}}. \quad (4.31)$$

Clearly solution three, the slow Alfvén wave, becomes unstable for

$$k < \frac{2V_o\gamma_o}{(\gamma_o^2 V_o^2 + d^2/\gamma_o^2)}. \quad (4.32)$$

Which for  $\gamma_o^2 V_o^2 \gg d^2/\gamma_o^2$  reduces to

$$k < \frac{2}{\gamma_o V_o},$$

giving in physical units

$$kV_o < 2\frac{\bar{\omega}_c}{\gamma_o} = 2\frac{\omega_c}{G(T)\gamma_o}. \quad (4.33)$$

Note how the temperature is manifested. For low temperatures  $G(T) \approx 1$  we recover the cold relativistic limit  $kV_o < 2\omega_c/\gamma_o$  [6]. The general condition, Eq. (4.33), gives the criterion for a relativistic temperature-dependent cyclotron or Alfvénic two-stream instability.

On the other hand, if  $d^2/\gamma_o^2 \gg V_o^2\gamma_o^2$ , which is a more appropriate limit for pulsar plasmas, Eq. (4.32) gives

$$kc < 2\frac{V_o}{c}\gamma_o^3\frac{\bar{\omega}_p^2}{\bar{\omega}_c}\left[1 - \frac{\gamma_o^4V_o^2}{d^2}G(T)\right] \approx 2\frac{V_o}{c}\gamma_o^3\frac{\omega_p^2}{\omega_c}. \quad (4.34)$$

Therefore in this particular limit the instability is not suppressed even at  $T \sim mc^2 \rightarrow G(T) \approx 4.37$ . The maximum growth rate for this instability (in the limit  $d^2/\gamma_o^2 \gg V_o^2\gamma_o^2$ ) is

$$Im(\omega)_{max} \approx \frac{V_o}{c}\gamma_o^2\frac{\omega_p^2}{\omega_c}. \quad (4.35)$$

Thus the growth rate is not suppressed by temperature effects (see Fig. 4.5).

At large  $k$ , the Alfvénic modes, Eqs. (4.28) are asymptotic to

$$\omega \approx kV_o \mp \frac{2}{\gamma_o}, \quad (4.36)$$

see Figs. 4.1-4.3, or in physical units to

$$\omega \approx kV_o \mp \frac{2\omega_c}{G(T)\gamma_o}. \quad (4.37)$$

Revealing temperature modifications to the cold limit result. We may call these relativistic temperature-dependent cyclotron waves.

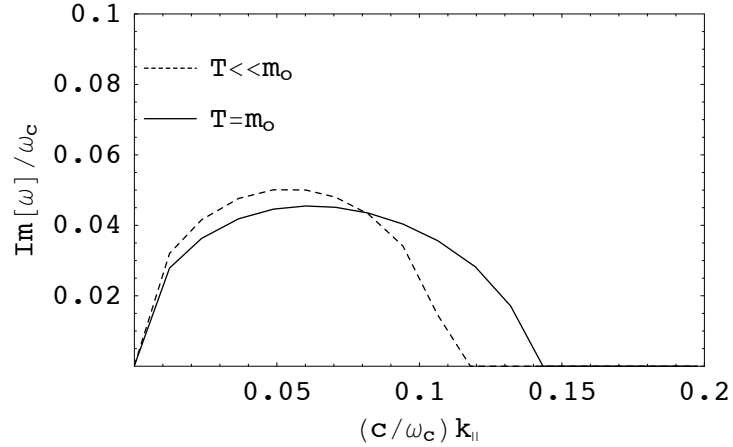


Figure 4.5: Numerical growth rate curves of the slow Alfvén mode, for various temperatures. Limit  $d^2/\gamma_o^2 \gg V_o^2\gamma_o^2$ . Note that, as explained in the text, for temperatures of the order of  $T \sim m_o$  the instability is not completely suppressed. With numerical parameters  $\gamma_o = 1.3, d = 4$ .

#### 4.2.1.1 Free energy source

At this point, it is important to comment on the energy source and type of instability. For an instability to be present, there has to be a “free” energy source that can drive it. As we have said above, the instability comes from the fact that we have an imaginary mode (the imaginary mode makes the factor  $-i\omega t$  positive and real, and, therefore, the amplitude  $\propto e^{-i\omega t}$  grows exponentially).

To track the origin of the unstable mode Eq. (4.35), we take a closer look at Eq. (4.31). There we see that that if  $V_o \rightarrow 0$ , the mode is positive and real, suppressing any possibility for a complex (or imaginary) mode. Therefore, the obvious source for the instability is the relative streaming between beams.

Although their velocities are equal and opposite, the total kinetic energy is not zero, that is

$$KE = \frac{1}{2}m_+V_+^2 + \frac{1}{2}m_-V_-^2 \quad (4.38)$$

$$= \frac{1}{2}m_o(-V_o)^2 + \frac{1}{2}m_o(+V_o)^2 \quad (4.39)$$

$$= m_oV_o^2 \neq 0. \quad (4.40)$$

This kinetic energy is the available free energy that transforms into wave excitation (see Sec. 5.4.1). Ultimately, as we have seen in Chapter 3, the relative streaming comes from the charge density deviations to screen the parallel electric field.

#### 4.2.1.2 Zero streaming limit ( $V_o \rightarrow 0$ )

If we go to the limit of no streaming (see Fig. 4.6), then the two EMP modes disappear, resulting in only one. Equations (4.24) and (4.27) remain valid but with  $\gamma_o \rightarrow 1$ . Note that the temperature effects still can bring down the cutoff as shown in Fig. 4.6.

On the other hand, for the Alfvénic modes, we find from Eq. (4.31)

$$\omega \approx \frac{kd}{(1+d^2)^{1/2}} \quad (4.41)$$

or in physical units

$$\omega \approx \frac{k\bar{V}_A}{(1+\bar{V}_A^2/c^2)^{1/2}} \quad (4.42)$$

the standard Alfvénic dispersion. This is why we called solutions three and four slow and fast Alfvénic modes. Note that in this limit the degeneracy

is lost. Yet temperature effects (in the limit  $\bar{V}_A < c$ ) can bring down the frequency, [remember  $\bar{V}_A = V_A/\sqrt{G(T)}$ ]; see Fig. 4.6.

In the large  $k$  limit, these Alfvénic modes [see Eq. (4.36)], are asymptotic to

$$\omega = \mp 2\bar{\omega}_c = \mp 2\frac{\omega_c}{G(T)} \quad (4.43)$$

the cyclotron frequency branch (see Fig. 4.6).

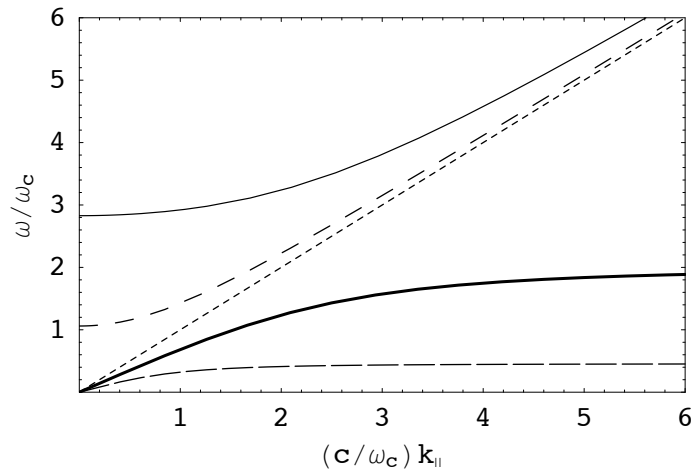


Figure 4.6: Dispersion curves for zero streaming ( $\gamma_o = 1, d = 1$ ). For temperatures:  $T \ll m_o$  (continues lines) and  $T = m_o$  (dashed lines). Notice the lowered cutoff of the EMP modes, and the frequency drop for the Alfvénic mode at  $T = m_o$ .

#### 4.2.2 Waves propagating perpendicular ( $\mathbf{k} \perp \hat{\mathbf{z}}$ )

For propagation perpendicular to the magnetic field ( $\theta = \pi/2$ ), Eq. (4.20) gives the dispersion relation

$$\left(\frac{1}{2} + \frac{1}{L}\right)^2 - \frac{1}{L^2} = 0 \quad (4.44)$$

for  $L = d^2(k^2 - \omega^2) \neq 0$ . Its solution is

$$\omega^2 = k^2 + \frac{4}{d^2} \quad (4.45)$$

or in physical units

$$\omega^2 = k^2 c^2 + \frac{4\omega_p^2}{G(T)}$$

the ordinary mode. Note that as the temperature increases the ordinary mode becomes a light wave (see Fig. 4.7). The fact that only the ordinary mode is present for  $\theta = \pi/2$ , is explained by looking at Eq. (4.13). It becomes

$$\omega \boldsymbol{\Omega}'_\alpha = 0 \Rightarrow \boldsymbol{\Omega}'_\alpha = 0 \quad (4.46)$$

therefore  $\mathbf{b} = -(\alpha/2)\nabla_\perp \times [\gamma_o \mathbf{v}_\alpha + \gamma_o^3(\mathbf{V}_o \cdot \mathbf{v}_\alpha)\mathbf{V}_o]$ , which, after substitution in Eq. (4.14) gives

$$(-\nabla_\perp^2 + \partial_t^2)\mathbf{b} = -\frac{4}{d^2}\mathbf{b} \quad \Rightarrow \quad \omega^2 = k^2 + \frac{4}{d^2} \quad (4.47)$$

after Fourier transform. The fact the perturbed vorticity is zero  $\boldsymbol{\Omega}'_\alpha = 0$  makes the magnetic field antiparallel with the sum of the vorticities (the curl of the current). Therefore the particles do not feel the ambient magnetic field.

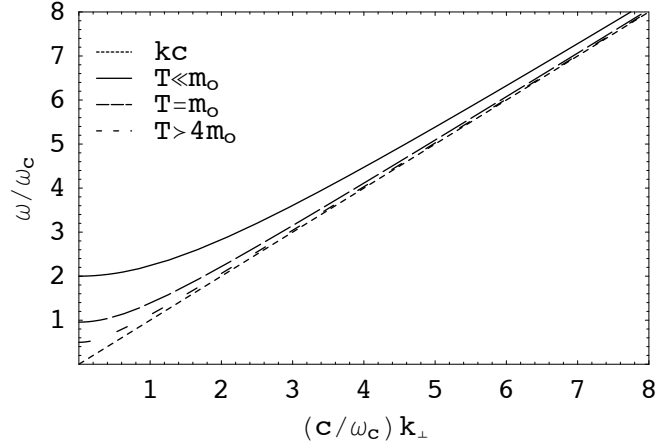


Figure 4.7: Dispersion curves for perpendicular propagation ( $\theta = \pi/2, d = 1$ ). Note how the increasing of temperature lowers the plasma cutoff until it reaches the asymptotic  $kc$  limit.

### 4.2.3 Waves propagating oblique ( $\theta = \pi/4$ )

For oblique propagation the determinant of Eq. (4.20) gives the dispersion relation

$$\begin{aligned}
0 = & \left\{ \frac{P^4 \gamma_o^8}{4} - \frac{P^2 \gamma_o^8}{2L^2} + \frac{\gamma_o^8}{4L^4} + \frac{P^4 \gamma_o^6}{2} - \frac{P^2 \gamma_o^6}{L^2} + \frac{\gamma_o^6}{2L^4} + \frac{P^4 \gamma_o^4}{4} - \frac{P^2 \gamma_o^4}{2L^2} \right. \\
& + \frac{\gamma_o^4}{2L^2(\omega - V_o k \cos \theta)(\omega + V_o k \cos \theta)} - \frac{P^2 \gamma_o^4}{4(\omega - V_o k \cos \theta)^2} - \frac{P^2 \gamma_o^4}{4(\omega + V_o k \cos \theta)^2} \\
& + \frac{\gamma_o^4}{4L^4} + \frac{\gamma_o^2}{2L^2(\omega - V_o k \cos \theta)(\omega + V_o k \cos \theta)} - \frac{P^2 \gamma_o^2}{4(\omega - V_o k \cos \theta)^2} - \frac{P^2 \gamma_o^2}{4(\omega + V_o k \cos \theta)^2} \\
& \left. + \frac{1}{4(\omega - V_o k \cos \theta)^2(\omega + V_o k \cos \theta)^2} \right\}. \quad (4.48)
\end{aligned}$$

Its solutions (four) are cumbersome, however the modes are similar to the parallel propagation case. We will describe them qualitatively with the help of Fig. 4.8. There we see four curves, two of them are EMP waves (degenerate)

just like in the parallel propagation case but with closer phase velocity. The other two are Alfvénic (or cyclotron in the large  $k$  region) modes that split into a fast and slow mode. The fast mode becomes subluminal at

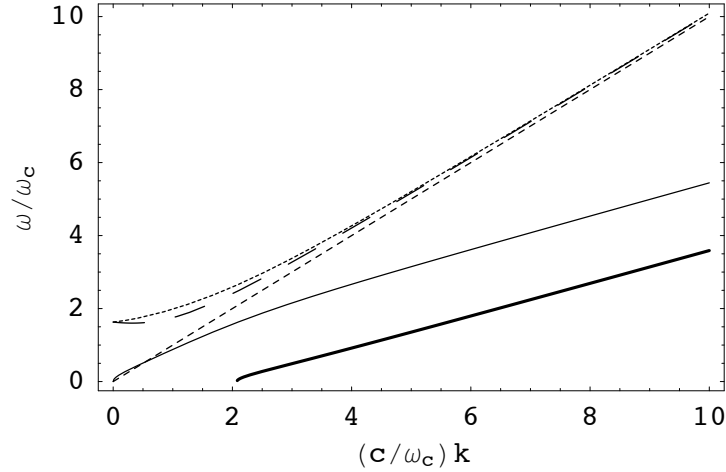


Figure 4.8: Dispersion curves for oblique propagation. Here we have four modes, two of them are EMP modes (short and long dashed lines). The slow branches (continues and thick lines) are the fast and slow Alfvénic modes respectively. Cold plasma ( $T \ll m_o$ ),  $\gamma_o = 1.3$ ,  $d = 2$ .

$$kc > 2(\omega_c/G)\sqrt{2(\gamma_o^2 - 1)/(1 + \gamma_o^2)^3},$$

which happens faster than in the parallel propagation case. The slow Alfvénic mode is cyclotron two-stream unstable at large wavelengths, just like in the parallel case. As temperature increases to  $T > m_o$  then we see that in fact the frequency decreases similarly to the parallel propagation case (see Fig. 4.9).

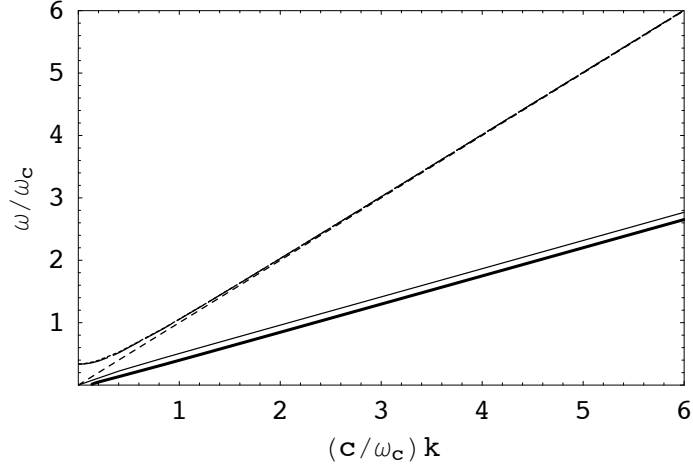


Figure 4.9: Dispersion curves for oblique propagation, for high temperatures  $T > m_o$  ( $\gamma_o = 1.3, d = 1.5$ ). Labeling same as in Fig. 4.8.

#### 4.2.4 Super strong magnetic field

It is always interesting to study propagating waves in the presence of super strong magnetic fields. Mathematically a super strong magnetic field is defined literally by  $B \rightarrow \infty$ , but as we have pointed out above, when the magnetic field is larger than  $B_{cr}$ , quantum effects play a major role. However we will take the approximation  $d \rightarrow \infty$  ( $d \equiv \omega_c/\omega_p$ ) to analyze dispersion relations, keeping in mind that our study can only be applicable for  $B < B_{cr}$ . We, therefore, proceed to study dispersion relations for two angles of propagation, parallel and oblique.

For strong magnetic fields and mildly relativistic velocities ( $\gamma_o = 4$ ) the parallel curves ( $\theta = 0$ ) are shown in Figs. 4.10-4.12. The modes appear as straight lines. To understand this, we take the  $d \rightarrow \infty$  limit of Eq. (4.22),

the EMP modes. After some algebra we find

$$\omega_{(2)}^{(1)} = \frac{1}{G} \left[ \frac{4}{\gamma_o^2} \mp \frac{4V_o}{\gamma_o} Gk + V_o^2 G^2 k^2 \right]^{1/2}. \quad (4.49)$$

Where  $G(T)$  has been written explicitly. It is not difficult to see that for small or large  $k$ ,  $\omega_2$  always gives

$$\omega_2 \approx \frac{2}{\gamma_o G} + V_o k. \quad (4.50)$$

For low temperatures ( $G \approx 1$ ) the cutoff (with the numerical values given to the plot) is at  $2/\gamma_o = 0.5$ , as shown in Fig. 4.10. Solution one on the other hand gives in the small  $k$  limit

$$\omega_1 \approx \frac{2}{\gamma_o G} - V_o k \quad (4.51)$$

i.e., same cutoff but negative slope (see Fig. 4.10). For large  $k$  it gives  $\omega_1 \approx V_o k$ . The other two transverse modes Eq. (4.28) (Alfvénic) have the following limits: solution four gives  $\omega_4 \approx k$  (for large and small  $k$ ) and solution three (the slow Alfvénic) gives

$$\omega_3 \approx \begin{cases} k & \text{if } k \lesssim 0.25 \\ \frac{2}{\gamma_o G} - V_o k & \text{if } 0.25 < k \lesssim 0.5 \\ -\frac{2}{\gamma_o G} + V_o k & \text{if } k \gtrsim 0.5 \end{cases} \quad (4.52)$$

Note that temperature effects, for all four modes in a strong magnetic field, are manifested through the terms  $\pm 2/[\gamma_o G(T)]$ . Thus as temperature rises both cutoffs (negative and positive) approach zero. Therefore the modes approach  $k$  (see Figs. 4.11 and 4.12). If  $G \approx 1$  we recover the cold plasma limit [6], as shown in Fig. 4.10. Note that the line along  $k$  ( $kc$  in physical units) is thus various lines very close together.

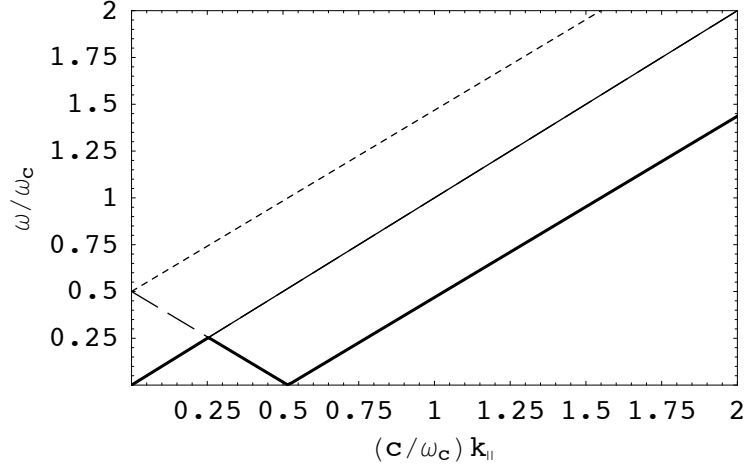


Figure 4.10: Dispersion curves for Parallel propagation. Super strong B field, cold plasma. The fast EMP mode (short dashed line) have dispersion  $\omega \approx 2/\gamma_o + V_o k$ . The slow Alfvén mode (thick solid line) is divided in three regions. The slow EMP (long dashed line) and fast Alfvén modes (continues line) have dispersion relations as described in the text. The numerical parameters  $\gamma_o = 4, d = 10^5$  were chosen for the sake of graphical clarity.

The case of oblique propagation with,  $\gamma_o = 10$  and strong magnetic field is shown in Fig. 4.13. There we see that the two EMP modes have become light waves and the Alfvén waves have become asymptotic to

$$\omega \approx \frac{1}{\sqrt{2}} kc \sqrt{2 - (V_o/c)^2}. \quad (4.53)$$

Note first that temperature effects are negligible in this particular limit. Secondly these waves do not reach the asymptotic limit of  $kc$  contrary to what happens for parallel propagation. The asymptotic value  $\omega \approx kc/\sqrt{2}$  (when  $V_o \rightarrow c$ ) is a geometric effect.

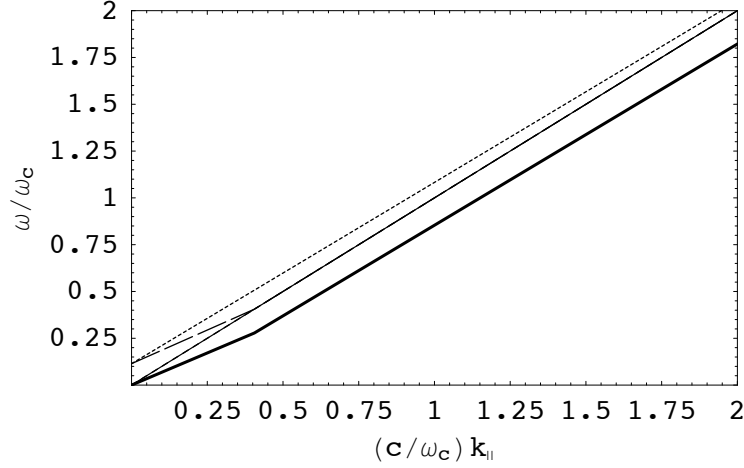


Figure 4.11: Dispersion curves for Parallel propagation. Strong B field. For  $T = m_o$ ,  $\gamma_o = 4$ ,  $d = 10^5$ . Notice the increase of temperature manifested through the decreasing cutoffs, making the curves approach the line  $kc$ . Labeling same as in Fig. 4.10.

### 4.3 Numerical estimates

To make numerical estimates, we will follow Refs. [11, 33] with the full realization that parameters at the polar caps are model dependent -there are several models, for example, for the generation of secondary pairs, leading to considerable uncertainties in the estimates of plasma density.

Our reference plasma is created outside a pulsar with a period  $P = 0.2$  s, and magnetic (dipole) field strength  $B_o = 10^{12}$  G; the corresponding density of corotation and cyclotron frequency are:  $n_{GJ} = 3.5 \times 10^{11} \text{ cm}^{-3}$ ,  $\omega_c = 1.75 \times 10^{19} \text{ s}^{-1}$ . The pair plasma (in the pulsar frame) has a density of the order of  $n_{\pm} = \Gamma n_{GJ}$  where  $\Gamma \approx 10^3 - 10^6$  is the multiplicity factor [11]. Note that the multiplicity factor is uncertain (see, e.g., [7]). The primary beam

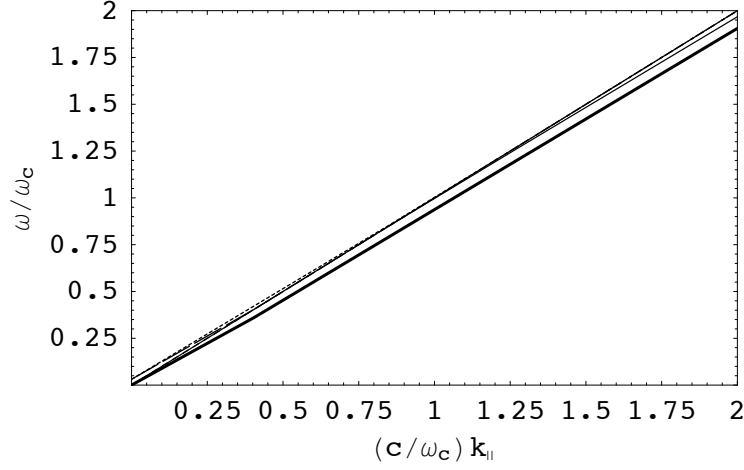


Figure 4.12: Dispersion for parallel propagation, for still higher temperatures  $T > m_o$ . Strong B field. Still  $\gamma_o = 4$ ,  $d = 10^5$ . Here the cutoffs  $\pm 2/[\gamma_o G(T)]$ , have become approximately zero and the curves have become virtually the line  $k$ . Labeling same as in Fig. 4.10.

has a density  $n_b$  equal to  $n_{GJ}$  at the time of pair creation [32], and flows along the open magnetic lines with energies  $\gamma_b \sim 10^7$ . The energy of the pair plasma particles is in the range  $\gamma_p \sim 10 - 10^3$ .

The pair plasma rest frame densities (in each plasma beam) are related to the density  $n_{GJ}$  (measured in the pulsar frame) via the multiplicity factor  $\Gamma$  and two Lorentz transformations: from the pulsar frame to the CM frame (with  $\gamma_p$ ) and from the CM to each component's rest frame (with  $\gamma_o$ ) that is  $n_o = \Gamma n_{GJ} / \gamma_p \gamma_o$  [11]. The corresponding plasma frequency (square of it) is  $\omega_p^2 = 1.11 \times 10^{21} - 10^{26} \text{ s}^{-2}$ .

For an instability to be a good candidate as a possible source of coherent radio emission generation, its growth rate  $[Im(w)]$ , evaluated at the pulsar

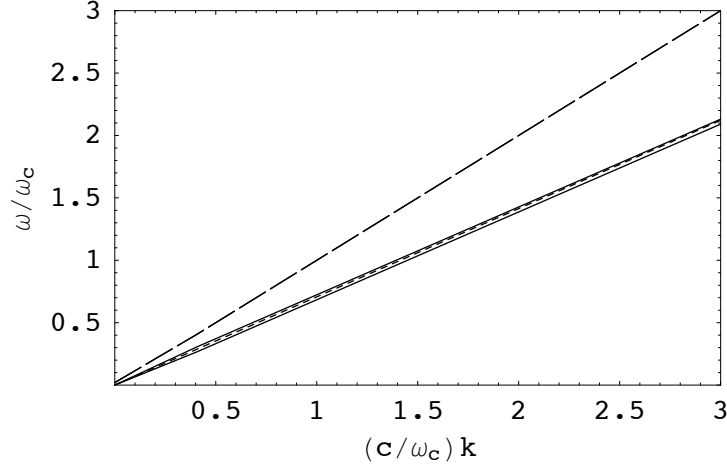


Figure 4.13: Dispersion curves for Oblique propagation. Strong B field. The EMP modes (long dashed line) have become asymptotically to  $kc$ . The Alfvénic modes (continuous and thick lines) have become asymptotically to  $kc/\sqrt{2}$  (short dashed line). With  $\gamma_o = 10, d = 10^5$ .

frame, should be much larger than the pulsar rotational frequency  $w = 2\pi/T \approx 31.4 \text{ s}^{-1}$ , that is

$$\frac{Im(\omega)}{\gamma_p} \gg w \quad (4.54)$$

where  $Im(\omega) = (V_o/c)\gamma_o^2(\omega_p^2/\omega_c)$ . We can then calculate the growth rate of this instability by assuming typical relative streaming energies  $\gamma_o$ . (i) For mildly relativistic streaming  $\gamma_o = 10$ , and the numerical parameters given above, we find the maximum growth rate to be

$$Im(\omega) \approx 6.2 \times 10^3 - 10^8 \text{ s}^{-1}. \quad (4.55)$$

(ii) For large relativistic streaming  $\gamma_o = 100$  we find

$$Im(\omega) \approx 6.3 \times 10^5 - 10^{10} \text{ s}^{-1}. \quad (4.56)$$

Therefore for case (i) and using  $\gamma_p = 10^3$ , we find

$$\frac{Im(\omega)}{\gamma_p} \approx 6.2 - 10^5 \text{ s}^{-1}, \quad (4.57)$$

whereas for (ii)

$$\frac{Im(\omega)}{\gamma_p} \approx 6.3 \times 10^2 - 10^7 \text{ s}^{-1} \gg 31.4 \text{ s}^{-1} \quad (4.58)$$

We see from the above that, for case (i), lower limit only, the instability is not fast enough. The second case is more attractive of course, since it is evident that the instability has the potential of being a good candidate for exciting waves or particles that could eventually help a nonlinear process to produce coherent emission.

#### 4.4 Summary and conclusions

We have considered propagation of relativistic waves in streaming magnetized plasmas. For parallel propagation we have four modes.

(1) For finite temperature and finite magnetic field the stable fast Alfvén wave is superluminal for large wavelengths only, becoming subluminal at  $k > 2(\omega_c/c)\sqrt{\gamma_o^2 - 1}$ . At large temperatures, however, it is always subluminal. In the super strong magnetic field case it has the vacuum dispersion relation.

- (2) The slow Alfvén wave is cyclotron two-stream unstable for large wavelengths and always subluminal. For temperatures of the order of  $T \sim m_o$  (and limit  $\gamma_o^2 V_o^2 \gg d^2/\gamma_o^2$ ) it is unstable. For ultra high temperatures it can be stabilized. However in the limit  $d^2/\gamma_o^2 \gg V_o^2 \gamma_o^2$  it is always unstable regardless of temperature. For strong magnetic field case it splits into three regions, with the dispersion relation  $\omega = -2/(\gamma_o G) + V_o k$  in the large  $k$  region.
- (3) The other two modes are degenerate electromagnetic plasmas waves which at high temperature become light waves.

For oblique propagation with strong magnetic field our dispersion relation is unaffected by temperature: it is valid in both cold and/or hot magnetized plasmas.

Because our model is incompressible, we find only the ordinary mode for perpendicular propagation; neither the pure streaming instability nor the compressional wave are permitted. Most relevant to radio emission theories is our result that the slow Alfvén wave is unstable, and is not fully stabilized even at temperatures of the order of  $T \sim m_o$ . In addition, for typical pulsar parameters, the calculated values show that the instability is quite fast and the waves can grow to such levels that the magnetic modulation could act as a wiggler. The pulsar's primary beam could interact with this wiggler and simulate a FEL (free electron laser) like effect, yielding coherent radiation. Detailed description of this is presented in the next chapter.

## Chapter 5

# Free Electron Lasers in Pulsar Magnetospheres

### 5.1 Introduction

The high brightness temperature associated with the radio emissions from pulsars signifies, as we will show, that the radiation mechanism must be coherent. Examples of coherent radiation can be found, for example, in lasers, where radiation is amplified by stimulated emission. Lasers are well known for their high intensity. The process responsible of such intensities is non-thermal.

Unlike lasers, a free electron laser (FEL) uses unbounded electrons to achieved the lasing effect. These free electrons, in the form of a beam, move through a periodic but static magnetic field, emitting synchrotron radiation. The synchronized interaction of these photons with the electrons gives rise to coherent radiation; the electrons give energy (feed) to the radiation field (photons).

Because of the FEL's large operation range, we will propose that, a FEL-like effect exists in pulsars. We will first describe the properties of the pulsar radio emissions, and then the basic concepts of FELs. Then we show that the interaction of the wiggler (the Alfvén wave) and the pulsar primary

beam may simulate a FEL effect and this could explain some of the characteristics of the pulsars radio emissions.

## 5.2 Pulsar's radiation

The radio flux density of pulsars (observed at 1.4 GHz) lies in the range  $20 \mu \text{ Jy}$  to  $5 \text{ Jy}$ . A Jansky ( $1 \text{ Jy} \equiv 10^{-23} \text{ erg s}^{-1} \text{ cm}^{-2} \text{ Hz}^{-1}$ ) is the standard flux density measure by radio telescopes. These radio emission fluxes are weak, however the associated intensities are not, as we will show it. This is because they are emitted from very small regions and at such low frequencies; the distances from which they are emitted, however, are not very far, relatively speaking (all pulsars detected reside in our own galaxy).

For example, suppose a pulsar is a sphere of radius  $R$  and it is at a distance  $d$  from us (the observer), see Fig. 5.1. Then the flux ( $F$ ) is given by [37]

$$F = \pi I \left( \frac{R}{d} \right)^2, \quad (5.1)$$

where  $I$  is the intensity or brightness. If the source were a black body radiator, then the intensity is given by

$$I = \frac{2h\nu^3/c^2}{e^{h\nu/k_B T} - 1}, \quad (5.2)$$

where  $h, \nu, T$  are, respectively, the Planck's constant, emitted frequency and temperature. At low frequencies ( $h\nu \ll k_B T$ ) Eq. (5.2) reduces to

$$I \approx \frac{\nu^2}{c^2} k_B T, \quad (5.3)$$

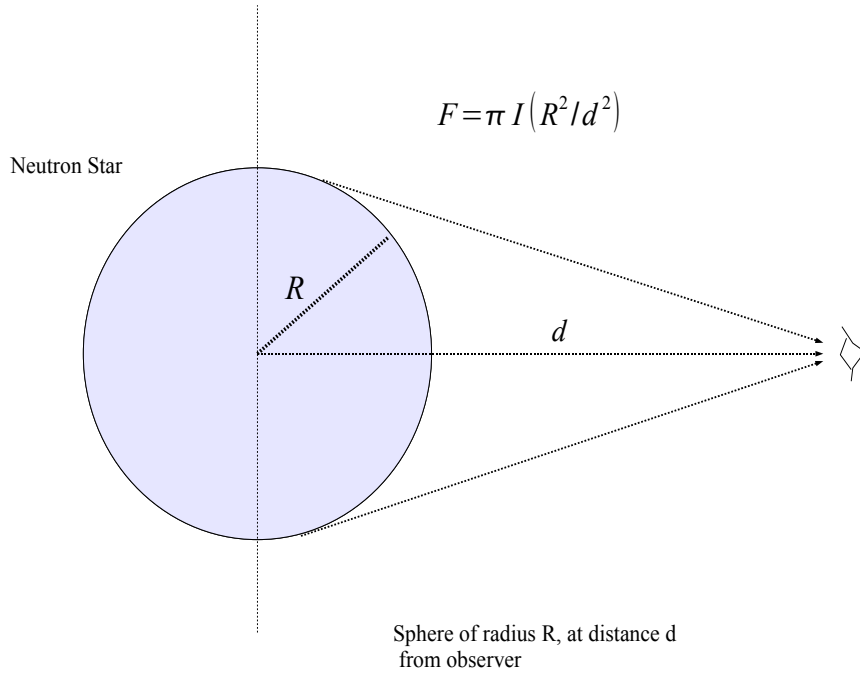


Figure 5.1: Sphere of radius  $R$ , at a distance  $d$

the Rayleigh-Jeans limit. Substitution of Eq. (5.3) into Eq. (5.1) gives us the brightness temperature of the source (in degrees Kelvin)

$$T = \frac{F c^2}{\pi k_B \nu^2 R^2} \approx 2 \times 10^{36} \frac{F d^2}{\nu^2 R^2} \text{ K}, \quad (5.4)$$

where we have used  $k_B = 1.38 \times 10^{-16} \text{ erg K}^{-1}$  for the Boltzmann's constant. Thus, for a neutron star of radius  $R = 10 \text{ km} = 10^6 \text{ cm}$ , at a distance  $d = 5 \text{ Kpc} \sim 15 \times 10^{21} \text{ cm}$ , with flux  $F = 5 \text{ Jy}$  and radio frequency  $\nu = 1.4 \text{ GHz}$  we obtain

$$T = 10^{28} \text{ K}. \quad (5.5)$$

For comparison, the temperature of the Sun's surface is  $\sim 6 \times 10^3$  K and the temperature of a Tokamak fusion device is  $\sim 10^8$  K. The energy, in electron volts (eV, where  $1\text{eV} = 10^4\text{K}$ ) associated with this temperature is  $10^{24}$  eV. In fact, we would have to go to the early epochs of the universe to reach such temperatures. For example, in the first  $10^{-35}$  s after the Big Bang, the temperature of the universe was  $10^{28}$  K (energies of  $10^{15}\text{GeV}$ ). Therefore, as we can see from the above examples, this temperature is, clearly, just too high.

This implies that the mechanism involved in the production of this radio emissions has to be a coherent effect; it cannot be a thermal source.

### 5.2.1 Coherence

Let us briefly recall the phenomenon of coherence. In a coherent process, the resulting radiation intensity is larger than the sum of the individual emitters' intensity. What we mean is, that normally when there is a random distribution of emitting particles, the total intensity is basically

$$I = \sum_{i=1}^N I_i \tag{5.6}$$

$$= I_1 + I_2 + I_3 + \dots \tag{5.7}$$

the sum of the  $N$  individual intensities (at a fixed frequency). The intensity is  $I \propto E^2$ , proportional to the square of the field amplitudes ( $E$ ). However, in a coherent radiative process, the size of the distribution of particles (also called bunches) is much smaller than the emitted wavelength. Then the individual

fields can add up

$$I = \left( \sum_{i=1}^N E_i \right)^2 \quad (5.8)$$

$$= (E_1 + E_2 + E_3 + \dots)^2, \quad (5.9)$$

increasing  $I$  dramatically [38]. Therefore in a spatial coherent process the fields, rather than the intensities, add. If  $N$  is the number of particles per bunch, then the resultant intensity is  $I \approx N^2 I_i$ . This coherent process is at the heart of the free electron laser's operation.

## 5.3 Free electron lasers

### 5.3.1 Operating principle

After the success of conventional lasers, a new type of coherent source appeared: the free electron laser or FEL. This new type of laser appeared from the beginning to be very promising, due to the peculiarity of its operating principles. Unlike conventional lasers, in a FEL the active medium is not made of atoms or molecules but, a beam of “free” electrons propagating at relativistic speeds through a static but periodic magnetic field called the undulator or wiggler. Where electrons experience a Lorentz force, they execute transverse oscillations and emit synchrotron radiation in the forward direction, see Fig. 5.2. Then, the synchronized interaction of the emitted radiation and electrons produces coherent radiation.

There are two basic types of FELs. On one of them, the photons emitted along the passage through the undulator are trapped in an optical

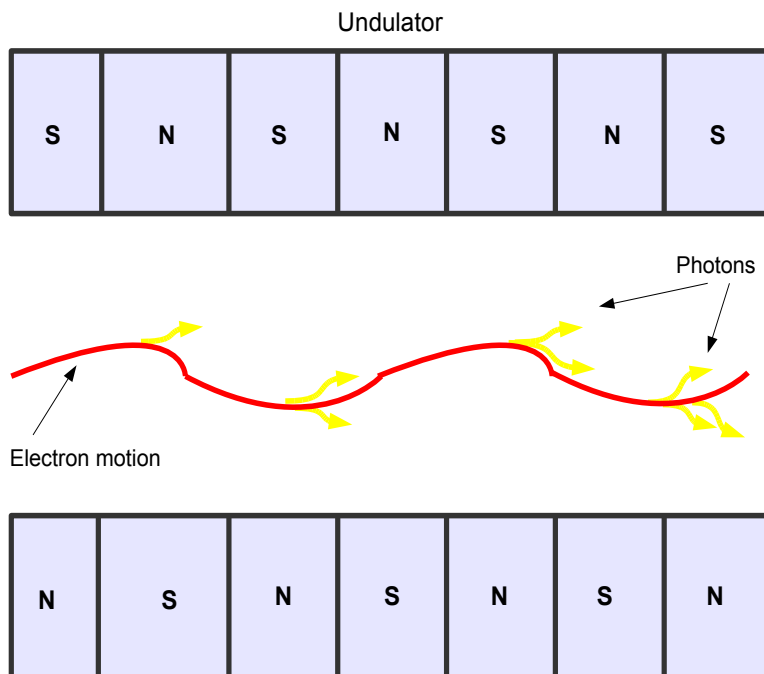


Figure 5.2: Free electron laser. The electron motion is on a plane perpendicular to the magnetic field lines.

cavity and then they interact again with a fresh electron beam. If the gain associated with this process is larger than the cavity losses, the laser action occurs. In full analogy with conventional lasers, when saturation is reached, highly coherent radiation can be extracted from the optical cavity, see Fig. 5.3

The other type, self-amplified spontaneous emission (SASE), is based on a different operation scheme, see Fig. 5.4. It is based on a single passage, which is possible if the electron beam “brightness” is good enough (high peak

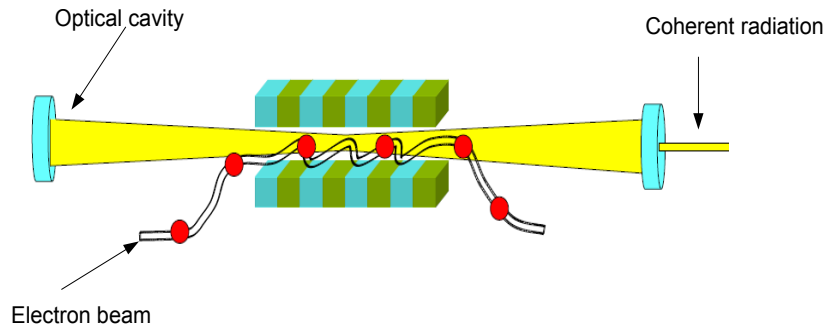


Figure 5.3: FEL, Optical cavity.

current) to have very high gain. In this operation mode, the electron beam interacts with its own spontaneous radiation producing coherent emission. It is this last operating scheme that we are interested in.

### 5.3.2 Electron motion in an undulator

In this section we will show the basics of an electron moving in the undulator. We will derive, for a given configuration, the condition for the resonant interaction between electrons and their emitted photons. On Fig. 5.5

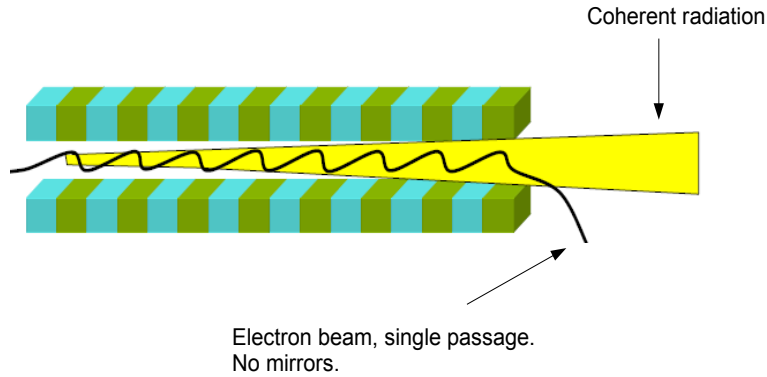


Figure 5.4: FEL SASE

we see a schematic picture of an electron moving through a static magnetic field. The electrons move in the  $z$  direction and the magnetic field varies with the spatial period  $\lambda_w$  in the longitudinal direction  $z$ . The magnetic field is

$$B_y = B_w \cos k_w z, \quad k_w = 2\pi/\lambda_w. \quad (5.10)$$

The electron moving at relativistic speeds, along the  $z$  direction, undergoes an undulating motion (oscillations) around the  $z$ -axis with the same spatial period as the transverse static magnetic field and perpendicular to it. Every time the orbit of the electron is bent, by the magnetic field, it emits synchrotron

radiation in the forward direction.

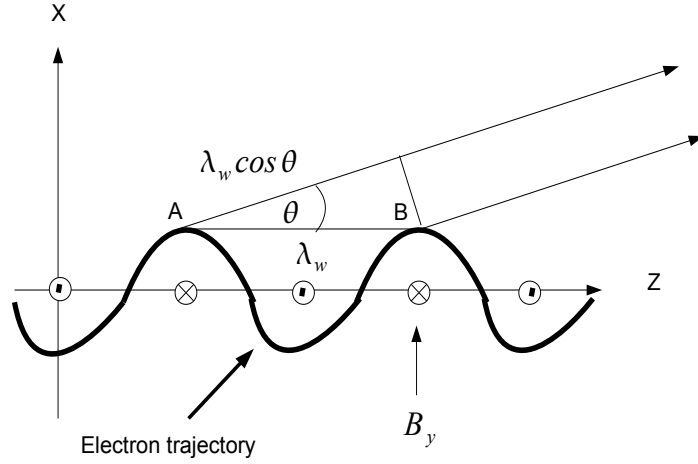


Figure 5.5: Schematic picture: electron motion in undulator

As seen on Fig. 5.5, suppose that the electron emits a pulse at point A, at time zero. The second pulse at point B, is emitted at time  $t_w = \lambda_w / \bar{v}_z$ , where  $\bar{v}_z$  is the electron's average velocity along  $z$ . For the two pulses to interfere constructively, the difference in the transit distance for the two pulses must be an integral multiple of the wavelength. Therefore

$$c \frac{\lambda_w}{\bar{v}_z} - \lambda_w \cos \theta = n \lambda_{FEL}, \quad n = 1, 2, 3 \dots \quad (5.11)$$

where  $\theta$  is the angle between the direction of the pulse propagation and the  $z$ -axis. In order to calculate the electron velocity  $\bar{v}_z$ , we need, first, to calculate the transverse velocity  $v_x$ . The equation of motion for a relativistic particle (electron) moving in a transverse magnetic field is,

$$m\gamma \frac{d\mathbf{v}_x}{dt} = -e(\mathbf{v}_z \times \mathbf{B}_y)/c = e(v_z/c)B_w \cos k_w z \hat{\mathbf{x}}, \quad (5.12)$$

where  $\gamma = 1/\sqrt{1 - v^2/c^2}$  and  $v = \sqrt{v_z^2 + v_x^2}$  is the magnitude of the electron's total velocity. Using  $v_z = dz/dt$  we can write Eq. (5.12) as

$$\frac{dv_x}{dt} = \frac{eB_w}{\gamma m_o c} \frac{dz}{dt} \cos k_w z, \quad (5.13)$$

which after integration becomes

$$v_x = \frac{eB_w}{\gamma m_o c k_w} \sin k_w z. \quad (5.14)$$

Therefore  $v_z$  becomes

$$\begin{aligned} v_z &= \sqrt{v^2 - v_x^2} \\ &= \left[ v^2 - \left( \frac{eB_w}{\gamma m_o c k_w} \right)^2 \sin^2 k_w z \right]^{1/2} \\ &\approx c \left\{ 1 - \frac{1}{2\gamma^2} \left[ 1 + \left( \frac{eB_w}{m_o c^2 k_w} \right)^2 \sin^2 k_w z \right] \right\}. \end{aligned}$$

Where we have used the fact that  $\gamma \gg 1$ . Averaging  $v_z$  with respect to  $z$  over one spatial period we get

$$\bar{v}_z = c \left[ 1 - \frac{1}{2\gamma^2} \left( 1 + \frac{1}{2} a^2 \right) \right] \quad (5.15)$$

where

$$a = \left( \frac{eB_w}{m_o c^2 k_w} \right). \quad (5.16)$$

If  $a \gg 1$  the undulator is called a wiggler. Substituting Eq. (5.15) in Eq. (5.11) we get (for the special case,  $n = 1$ ) in the limit  $\theta \ll 1$

$$\lambda_{FEL} \approx \frac{\lambda_w}{2\gamma^2} \left( 1 + \frac{1}{2}a^2 \right), \quad (5.17)$$

the corresponding frequency is

$$\omega_{FEL} = \frac{2\gamma^2 \omega_w}{\left( 1 + \frac{1}{2}a^2 \right)}, \quad \omega_w = \bar{v}_z k_w. \quad (5.18)$$

Equation (5.18) is the radiation frequency associated if two emitted pulses were to interfere constructively. We have called it FEL frequency, because it is exactly the frequency at which the resonant electrons will give energy to the plane wave formed by the synchrotron photons; the photons are polarized in the same plane as the plane motion of the electrons, they can be considered to form a plane wave. For example, the plane wave will be polarized (electric field) in the  $x$ -plane, and since the transverse velocity of the electrons is  $v_x$ , there can be exchanged of energy between the two as will be seen.

### 5.3.3 Energy exchange and condition for resonant interaction

A plane electromagnetic (EM) wave, traveling along  $z$ , may be written as

$$E_x = E_o \sin(\omega t - kz + \psi) \quad (5.19)$$

$$B_y = B_o \sin(\omega t - kz + \psi), \quad (5.20)$$

where  $\psi$  ( $E_o$ ) denote a constant phase (amplitude) of the electric field. The energy transfer from an electron to the light wave is given by

$$\frac{dK_E}{dt} = \frac{d}{dt}[m_o c^2(\gamma - 1)] = -ev_x E_x, \quad (5.21)$$

which, after using, Eq. (5.14) becomes

$$\begin{aligned} \frac{dK_E}{dt} &= -\frac{e^2 B_w E_o}{\gamma m_o c k_w} \sin k_w z \sin(\omega t - kz + \psi) \\ &= -\frac{e^2 B_w E_o}{\gamma m_o c k_w} \{ \cos[\omega t - (k + k_w)z + \psi] - \cos[\omega t - (k - k_w)z + \psi] \} \\ &\equiv -\frac{ec a E_o}{\gamma} (\cos \phi + \cos \chi), \end{aligned} \quad (5.22)$$

where we have used the definition of  $a$ , and introduced the following notation

$$\phi = [\omega t - (k + k_w)z + \psi], \quad \chi = [\omega t - (k - k_w)z + \psi]. \quad (5.23)$$

$\phi$  is called the ponderomotive phase, and  $\chi$  is a rapidly oscillating phase that averages to zero.

The condition for continuous energy transfer from electron to the electromagnetic wave is

$$\frac{dK_E}{dt} < 0 \implies \phi = \text{constant}, \quad (5.24)$$

with optimum value  $\phi = 0$ . The condition  $\phi = \text{constant}$  can only be fulfilled for a certain wavelength

$$\begin{aligned} \phi(t) &= \omega t - (k + k_w)\bar{v}_z t + \psi = \text{const.} \implies \\ \frac{d\phi}{dt} &= \omega - (k + k_w)\bar{v}_z = 0, \end{aligned} \quad (5.25)$$

where we have used the approximation  $v_z \approx \bar{v}_z$ . Therefore

$$\frac{\omega}{k + k_w} = \frac{kc}{k + k_w} = \bar{v}_z, \quad (5.26)$$

is the resonant condition necessary for energy exchange from the electrons to the EM wave. In words, the interaction of the plane EM wave with the static magnetic field has created a beat wave with same frequency but with wave number equal to the sum of the EM wave and the static magnetic field, making the beat wave's phase velocity smaller than  $c$  and therefore the electrons (that move at speeds less than  $c$ ) can interact with it. From Eq. (5.26) and using Eq. (5.15) we arrive at

$$\lambda = \frac{\lambda_w}{2\gamma^2} \left( 1 + \frac{1}{2}a^2 \right), \quad (5.27)$$

which is the precisely the condition for two emitted pulses to interfere constructively. What about  $\chi$ ? well, it can be written as  $\cos \chi = \cos(\phi - 2k_w z) \propto \cos(2k_w z)$  which averages to zero ( $\phi = \text{constant}$ ). Therefore the lasing process in the undulator is started by an electromagnetic wave of wavelength  $\lambda_l$  and resonant electrons with energy  $E_R = \gamma_R m_o c^2$  defined by

$$\lambda_l = \frac{\lambda_w}{2\gamma_R^2} \left( 1 + \frac{a^2}{2} \right), \quad (5.28)$$

or

$$\gamma_R = \sqrt{\frac{\lambda_u}{2\lambda_l} \left( 1 + \frac{a^2}{2} \right)}. \quad (5.29)$$

Therefore, electrons with energy  $E = E_R$  ( $\gamma = \gamma_R$ ) emit radiation with wavelength  $\lambda = \lambda_l$ .

### 5.3.4 Gain and electron beam requirements

Because of our obvious physical constraints, we are interested, as explained above, in the FEL SASE.

SASE is possible if the electron beam has a high peak current. The gain, which characterizes the device, is given by [38]

$$g \sim \frac{j a^2}{\gamma^3 I_a k_w^2}, \quad (5.30)$$

where  $j$  is the electron beam current density,  $\gamma$  is the Lorentz factor for the electrons,  $k_w = 2\pi/\lambda_w$  and  $I_a$  is a constant current,  $I_a = (m_e c/\mu_o e) \approx 10^3 \text{ A} = 10^{12} \text{ statAmps}$ . The radiation intensity  $I$  initially grows exponentially along the undulator,

$$I = I_o \exp[z/L_g], \quad (5.31)$$

until it saturates.  $I_o$  is the starting intensity and  $L_g$  is the gain length given by

$$L_g = \frac{\lambda_w}{4\pi\sqrt{3}\rho}. \quad (5.32)$$

The FEL parameter,  $\rho$ , is the key dimensionless parameter that characterizes the performance of a SASE device [38]

$$\rho = g^{1/3} \sim \frac{j^{1/3} a^{2/3}}{10^4 \gamma k_w^{2/3}}. \quad (5.33)$$

The number of undulator periods is given by  $N_w = L_g/\lambda_w$ . In laboratory experiments, unlike our case, to reduce the overall undulator length, the gain length  $L_g$  must be made as short as possible.

During the FEL amplification region, energy is transferred from the electron beam to the radiation field. The amplification stops when the device has reached saturation. The FEL depends linearly, as we have seen above, on the input power  $I_o$  during the exponential regime. However, saturation power is independent of the input power

$$P_{sat} = \rho P_{beam}, \quad (5.34)$$

that is, it only depends on the beam power (see Fig. 5.6). The saturation length is approximately

$$L_{sat} \approx \lambda_w / \rho = L_g. \quad (5.35)$$

## 5.4 FEL in pulsar magnetospheres

We have shown in Sec. 4.2.1, that under well-defined conditions a cyclotron (or Alfvénic) two-stream instability exists at pulsar polar cap plasmas. Since a highly energetic charged (the primary) beam penetrates those plasmas, the interaction of this with the unstable mode could simulate an FEL-like effect. First, we will calculate the frequency range radiated from the FEL, and then we compare the obtained results with the observed frequencies. Second, we will calculate the power emitted and compare it to the observed luminosities from the pulsar radiation. All of the above will be carry out doing numerical estimates only. For example, we do not know the exact polarization of the Alfvénic mode or its magnitude, however we know that it is a shear (transverse polarized) Alfvénic mode propagating along the mag-

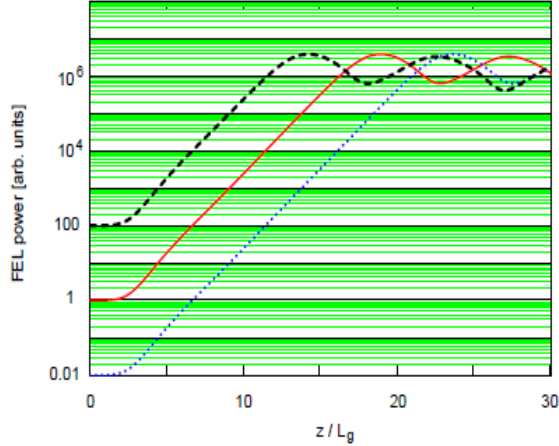


Figure 5.6: FEL saturation. The power depends linearly on the input power (exponential regime). However the saturation power is independent on the input power. Taken from “FEL Theory for Pedestrians” by Peter Schmuser.

netic field lines ( $z$ -direction). The primary beam also propagates along  $z$ . Although the condition  $\mathbf{E} \cdot \mathbf{B} \neq 0$  exists near the surface of the pulsar, the pulsar standard model assumes that in the pair plasma region  $\mathbf{E} \cdot \mathbf{B} = 0$ , as we explained in Sec. 3.2.2. In what follows below, we work in the plasma frame, and only the final results will be transformed to the pulsar frame.

We will use the following reference pulsar parameters:  $\omega_p^2 = 10^{22}\text{s}^{-2}$  [plasma frequency (square of it)].  $\omega_c = 10^{19}\text{s}^{-1}$  (cyclotron frequency).  $\gamma_b = 10^7$  (primary beam Lorentz factor).  $\gamma_P = 10^3$  [plasma Lorentz factor (CM)].  $\gamma_o = 10^2$  [pair’s beams Lorentz factor (w.r.t. CM)].  $n_{GJ} = 3.5 \times 10^{11}\text{cm}^{-3}$  (corotating

density).  $n_{\pm} = \Gamma n_{GJ}/\gamma_p\gamma_o$  (pair plasma density).  $\Gamma = 10^6$  (multiplication factor).  $\gamma'_b \sim \gamma_b/\gamma_p = 10^4$  (primary beam Lorentz factor measure in the plasma frame).

### 5.4.1 Frequency

The FEL (emitted) frequency is given by

$$\omega_{FEL} = \frac{2\gamma_b'^2 k_w c}{\left(1 + \frac{a^2}{2}\right)}, \quad (5.36)$$

where the dimensionless parameter

$$a = \frac{eB_w}{m_o c} \frac{1}{k_w c} = \frac{\omega_w}{k_w c}$$

depends on the wiggler amplitude  $B_w$  and the wiggler wave vector  $k_w$ . More explicitly, the emission frequency ( $\nu = \omega/2\pi$ ) is

$$\nu_{FEL} = 5.6 \times 10^{24} \frac{k_w^2}{B_w^2} \text{ Hz}, \quad (5.37)$$

where we have used the fact  $a \gg 1$ . To calculate the frequency we must estimate the relevant  $B_w$  and  $k_w$ .

In the linear theory the instability is driven by the relative streaming between positrons and electrons (see Sec. 4.2.1.1).  $B_w$  the perturbed amplitude or magnetic modulation, is not known. Therefore, a rough estimate for  $B_w$  may be made by equating the streaming free energy to the magnetic energy. We find ( $\sigma = 0.1$ )

$$\sigma n_{\pm} m_e c^2 (\gamma_o - 1) = \frac{B_w^2}{8\pi} \Rightarrow B_w \approx 2.7 \times 10^4 \text{ G}. \quad (5.38)$$

Where  $\sigma$  is a numerical constant that parametrizes the energy conversion formula, for example, for a full conversion ( $\sigma = 1$ )  $B_w \approx 8.5 \times 10^4 \text{G}$ .

To estimate  $k_w$ , we have the  $\Delta k$  region given by Eq. (4.34), where the wave is unstable,

$$k_w \leq \Delta k = 2 \frac{V_o}{c^2} \gamma_o^3 \frac{\omega_p^2}{\omega_c} = 0.066 \text{ cm}^{-1}. \quad (5.39)$$

Substituting the numerical values of Eqs. (5.38)-(5.39) in Eq. (5.37), we get for the frequency (at the pulsar frame)

$$\nu_{FEL}^p = \frac{\nu_{FEL}}{\gamma_p} \leq 3.36 \times 10^{10} \text{ Hz} = 33.6 \text{ GHz}, \quad (5.40)$$

this limit does correspond to the typical observed frequencies of pulsar radio emissions. Since, in principle,  $\Delta k$  can go to zero, therefore setting the lower frequency limit to Eq. (5.40) will eventually depend on: the saturation length  $L_{sat}$ , the maximum streaming energy transfer to magnetic modulation or ultimately by the pulsar observational frequency constraints. We can, for example, calculate the corresponding FEL frequency when the growth rate (instability) is maximum [see Eq. (4.35)], that is,  $k_w = k_{max} = \Delta k/2$

$$\nu_{FEL}^p = 8.4 \text{ GHz}, \quad (5.41)$$

which is in good agreement with pulsar's emission frequencies .

### 5.4.2 Power

As we mentioned in the introduction, the observed pulsar luminosities lie in the range  $10^{22} - 10^{28} \text{ erg s}^{-1}$ . In order to calculate power emitted by

FEL, we will assume that it has reached the saturation state. As we have explained earlier, the saturation power does not depend on the input power, but only on the beam power and the saturation parameter. That is,

$$P_T = \rho \times P_{beam} . \quad (5.42)$$

Where  $\rho$  is the saturation parameter and

$$P_{beam} = An_b c \gamma_b m c^2 \quad (5.43)$$

is the beam power. Where  $n_b \approx n_{GJ}$ ,  $\gamma_b = 10^7$  and  $A$  is the beam area or cross section. Assuming typical parameters, [see Eq. (3.15) and Fig. 3.2], we get

$$A \sim 10^8 \text{ cm}^2 ,$$

that is, a fraction of the pulsar's polar area. Combining the primary beam power

$$P_{beam} = 10^{30} \text{ erg s}^{-1} . \quad (5.44)$$

and the saturation parameter (for  $k_w = \Delta k / 2 = 0.033 \text{ cm}^{-1}$ )

$$\rho = \frac{j_b^{1/3} a^{2/3}}{10^4 \gamma_b' k_w^{2/3}} \sim 0.01$$

the total power emitted is

$$P_T \sim 10^{28} \text{ erg s}^{-1} . \quad (5.45)$$

Which is very much in the observed luminosities range. Note that, the power at the plasma and pulsar frame is the same since power is an invariant. The value used for  $k_w$ , is the value at which the growth rate (instability), Eq. (4.35), is maximum.

## 5.5 Discussion

As we have seen above, the estimated values for the frequency and power emitted are within the range of the expected values for a typical pulsar. Of course there are still open questions. For example, is the saturation mechanism for the FEL achievable in these magnetospheric circumstances? How much does the primary beam need to travel before reaching saturation? And how does that compare with the dimensions of the pulsar magnetospheres?

We can only answer some of these questions. For example, we can estimate the saturation length of the primary beam using Eq. (5.35), which for  $k_w = 0.033 \text{ cm}^{-1}$  yields

$$L_{sat} = \lambda_w / \rho \approx 1.8 \times 10^4 \text{ cm}. \quad (5.46)$$

$L_{sat}$  is a short enough distance for the primary beam to achieve saturation before, for example, reaching the light cylinder surface [see Eq. (3.8)]. A reasonable saturation mechanism can also be imagined: when the amplitude of the wave increases, the particles will eventually get trapped by the wave. The energy is pumped back and forth between particles and the wave reaching saturation. We have not yet found, within the pulsar context, an analytical explanation for this but it is something that we will work on in the future.

## Chapter 6

### Exact solutions: nonlinear waves

#### 6.1 Introduction

In this final chapter we will study an interesting property of the relativistic fluid model introduced in Chapter 2. This property allows for exact solutions. The essence of these solutions lie in the arbitrary amplitudes of the perturbed fluctuating fields. In previous chapters, when studying dispersion relations, we have assumed that the fluctuating quantities are smaller than the system's equilibrium.

It is well known (see Appendix) that the exact solution to the incompressible ideal magnetohydrodynamics (MHD), the non-linear Alfvén wave has found use in all studies of Alfvénic turbulence in astrophysical situations. The essence of this solution lies in the arbitrary amplitudes of the perturbed fluctuating fields with the requirement  $\mathbf{v} = \pm\alpha\mathbf{b}$ , where  $\alpha = V_A/B_o$ . In fact spacecraft measurements [39], such as the ones obtained by the Mariner-II in the year 1962, indicate that in the interplanetary medium a high degree of correlation exists between the fluctuating plasma fluid velocity  $\mathbf{v}$  and the fluctuating magnetic field  $\mathbf{b}$ .

Recently it has been found [40] that the Hall MHD allows for exact

solutions too. In fact the Hall MHD solutions are a set of one-parameter, three-dimensional, time-dependent states. These states, with the appearance of propagating plane waves, are exact nonlinear solutions that subsume, in the long wave limit, the Alfvénic states of MHD.

Here we generalized these modes by relaxing the Hall MHD assumptions, that is, the masses are now arbitrary forming a two fluid relativistic system. We find that the dispersion relation is amplitude dependent and we proceed onto analyzing its consequences.

## 6.2 Relativistic nonlinear two-fluid waves

Let us re-write here, Eqs. (2.7) and (2.12)

$$\frac{\partial \boldsymbol{\Omega}_{\pm}}{\partial t} = \nabla \times (\mathbf{V}_{\pm} \times \boldsymbol{\Omega}_{\pm}), \quad (6.1)$$

$$\nabla \times (\nabla \times \mathbf{B}) + \frac{\partial^2 \mathbf{B}}{\partial t^2} = \frac{c^2}{V_A^2} \nabla \times [\gamma_+ \mathbf{V}_+ - \gamma_- \mathbf{V}_-], \quad (6.2)$$

where, as usual

$$\boldsymbol{\Omega}_{\pm} \equiv \mathbf{B} \pm \mu_{\pm} \nabla \times \gamma_{\pm} \mathbf{V}_{\pm} \quad (6.3)$$

is the generalized vorticity. The normalizations are the same as those used in Chapter 2. To look for waves we, as usual, decompose

$$\mathbf{B} = \hat{e}_s + \mathbf{b} \quad (6.4a)$$

$$\mathbf{V}_{\pm} = \mathbf{v}_{\pm}, \quad (6.4b)$$

where  $\hat{e}_s$  is the unit vector along the ambient field  $B_o$ . Note that there is not an ambient flow and  $\mathbf{v}$  and  $\mathbf{b}$  are fluctuating quantities of arbitrary magnitude. Equations (6.4a) and (6.4b) will convert Eqs. (6.1) and (6.3) to

$$\frac{\partial}{\partial t} \boldsymbol{\omega}_{\pm} = \nabla \times (\mathbf{v}_{\pm} \times \hat{e}_s) + \nabla \times (\mathbf{v}_{\pm} \times \boldsymbol{\omega}_{\pm}), \quad (6.5)$$

where

$$\boldsymbol{\omega}_{\pm} = \mathbf{b} \pm \mu_{\pm} \nabla \times \gamma_{\pm} \mathbf{v}_{\pm}. \quad (6.6)$$

Since  $\mathbf{v}$  and  $\mathbf{b}$  are not assumed to be small quantities, then, to find (exact) solutions to Eq. (6.5) we use

$$\begin{aligned} \mathbf{v}_{\pm} &= \alpha_{\pm} \boldsymbol{\omega}_{\pm} \\ &= \alpha_{\pm} (\mathbf{b} \pm \mu_{\pm} \nabla \times \gamma_{\pm} \mathbf{v}_{\pm}), \end{aligned} \quad (6.7)$$

with  $\alpha_{\pm}$  as separation constants. Therefore Eq. (6.5) becomes

$$\frac{\partial}{\partial t} \mathbf{v}_{\pm} = \alpha_{\pm} \nabla \times (\mathbf{v}_{\pm} \times \hat{e}_s) = \alpha_{\pm} (\hat{e}_s \cdot \nabla) \mathbf{v}_{\pm}, \quad (6.8)$$

where we have used  $\nabla \cdot \mathbf{v}_{\pm} = 0$ .

Equation (6.7) was obtained to remove the nonlinear terms from Eq. (6.5). However, one immediately notices that, the system of Eqs. (6.7)-(6.8) is not quite yet linear because the inherent nonlinearity introduced by the  $\gamma$  factor. The original nonlinear system, thus, is not broken into a series of linear equations.

Fortunately, we can analytically solve the nonlinear system embodied in Eqs. (6.7)-(6.8); the properties associated with circular-polarization are the

basic ingredients which allow a solution [40]. To proceed, let us assume that  $\alpha_+ = \alpha_- = \alpha$ , then Eq. (6.8) allows the wave-like solution

$$\mathbf{v}_{\pm}(\mathbf{r}, t) = \hat{v}_{\pm} \exp[i(\mathbf{k} \cdot \mathbf{r} + \alpha \hat{e}_s \cdot \mathbf{k} t)], \quad (6.9)$$

where  $\hat{v}_{\pm}$  are constant vectors. However, if for arbitrary  $\hat{v}_{\pm}$ , we try to calculate  $\gamma_{\pm} = (1 - |\mathbf{v}_{\pm}|^2)^{-1/2}$ , it will be a function of space and time, and in that case Eq. (6.9) cannot be a simultaneously solution of Eq. (6.7). There is one special case when Eq. (6.9) can be, when

$$\hat{v}_{\pm} = A_{\pm} [\hat{e}_x + i \hat{e}_y], \quad (6.10)$$

or some equivalent circular polarization. If Eq. (6.10) is valid, it is straightforward to show that

$$\gamma_{\pm} = \frac{1}{(1 - |\mathbf{v}_{\pm}|^2)^{1/2}} = \frac{1}{(1 - A_{\pm}^2)^{1/2}}, \quad (6.11)$$

which is independent of space time. We are still not through since,

$$\nabla \times \gamma \mathbf{v} \sim \frac{A}{(1 - A^2)^{1/2}} \nabla \times [\hat{e}_x + i \hat{e}_y] e^{i\mathbf{k} \cdot \mathbf{r}} = \frac{A e^{i\mathbf{k} \cdot \mathbf{r}}}{(1 - A^2)^{1/2}} i \mathbf{k} \times [\hat{e}_x + i \hat{e}_y]$$

will be proportional to  $[\hat{e}_x + i \hat{e}_y]$  if and only if  $\mathbf{k} = k \hat{e}_z$ , that is the wave propagates along  $z$  while the fluctuations are circularly polarized in the plane perpendicular to propagation. With this realization, we then find that our problem is fully solved with:

$$\mathbf{v}_{\pm} = A_{\pm} [\hat{e}_x + i \hat{e}_y] e^{i(kz + \alpha \hat{e}_s \cdot \hat{e}_z kt)} \quad (6.12)$$

$$\mathbf{b} = q [\hat{e}_x + i \hat{e}_y] e^{i(kz + \alpha \hat{e}_s \cdot \hat{e}_z kt)}, \quad (6.13)$$

where  $A_{\pm}$  and  $q$  are related through Eqs. (6.7) and (6.2) which become three algebraic equations

$$\frac{A_+}{\alpha} = q + \mu_+ \frac{kA_+}{(1 - A_+^2)^{1/2}} \quad (6.14a)$$

$$\frac{A_-}{\alpha} = q - \mu_- \frac{kA_-}{(1 - A_-^2)^{1/2}} \quad (6.14b)$$

$$k^2 [1 - \alpha^2(\hat{e}_s \cdot \hat{e}_z)^2] q = \frac{k}{d^2} \left[ \frac{A_+}{(1 - A_+^2)^{1/2}} - \frac{A_-}{(1 - A_-^2)^{1/2}} \right]. \quad (6.14c)$$

where  $d \equiv V_A/c$ . The system of Eqs. (6.14a)-(6.14c) is nonlinear. In the nonrelativistic limit ( $A_{\pm}^2 \ll 1$ ) the system becomes linear, and we get the following dispersion relation which does not depend on the field amplitudes

$$[1 - \alpha^2(\hat{e}_s \cdot \hat{e}_z)^2] (1 - \alpha k \mu_+)(1 + \alpha k \mu_-) = \alpha^2/d^2. \quad (6.15)$$

Equation (6.15) can be solved for  $\alpha = \alpha(k)$ , remembering that, the frequency is  $\omega = -\alpha k(\hat{e}_s \cdot \hat{e}_z)$ . For the relativistic case, however, an amplitude-independent dispersion relation is not possible.

### 6.3 Solution to the nonlinear equations

The relativistic system embodied in Eqs. (6.14a)-(6.14c) is numerically solved, by finding  $\omega$  as a function of  $k$  and only one of the amplitudes ( $A_+$ ), i.e.,  $\omega = \omega(k, A_+)$ . We have investigated two cases: plasma with different species and plasma with same species (pair plasma). The results are shown in Figs. 6.1-6.7. In what follows we explain the numerical results physically and, whenever possible, analytically. We restrict ourselves to the cold plasma

case only,  $G(z_{\pm}) \approx 1 \Rightarrow \bar{m}_{\pm} \approx m_o$ , and to (anti) parallel  $\hat{e}_s \cdot \hat{e}_z = (-) + 1$  propagation only.

### 6.3.1 Different species $\mu_+ \rightarrow 1, \mu_- \rightarrow 0$

#### 6.3.1.1 Non-relativistic case ( $A_{\pm}^2 \ll 1$ )

The numerical results for this case are shown in Fig. 6.1. There we see two plots. One is the Whistler mode (light-blue color) and the other (light-red color) is the cyclotron branch. Of course, both modes, become the Alfvénic wave at sufficiently small  $k$ . These modes can be easily understood from Eq. (6.15) which in the above limits reduces to  $[(\hat{e}_s \cdot \hat{e}_z)^2 = 1]$

$$(1 - \alpha^2)(1 - \alpha k) \approx \alpha^2/d^2. \quad (6.16)$$

For small  $k$  it gives

$$1 - \alpha^2 \approx \alpha^2/d^2, \quad (6.17)$$

or

$$\alpha = \pm \frac{d}{\sqrt{1 + d^2}}. \quad (6.18)$$

After using  $\omega = -\alpha k(\hat{e}_s \cdot \hat{e}_z)$  we find

$$\omega = \pm \frac{d}{\sqrt{1 + d^2}} k = \pm \frac{V_A/c}{\sqrt{1 + (V_A/c)^2}} k(\hat{e}_s \cdot \hat{e}_z) \quad (6.19)$$

reproducing the MHD Alfvénic relationship for both the parallel and antiparallel propagating waves. If  $V_A < c$  then Eq. (6.19) gives (in physical units)

$$\frac{\omega}{\omega_c} = \frac{V_A}{c} \left( \frac{c}{\omega_c} \right) k \Rightarrow \omega = V_A k(\hat{e}_s \cdot \hat{e}_z). \quad (6.20)$$

Likewise if  $V_A > c$  Eq. (6.19) gives

$$\omega = ck(\hat{e}_s \cdot \hat{e}_z). \quad (6.21)$$

In the large  $k$  limit Eq. (6.16) gives us

$$(1 - \alpha k) \approx \alpha^2/d^2 \Rightarrow \alpha \approx -kd^2 \quad (6.22)$$

for  $d \ll 1$ , and

$$(1 - \alpha k) \approx 0 \Rightarrow \alpha = \frac{1}{k} \quad (6.23)$$

for  $d \sim 1$ . These limits correspond to the Whistler

$$\omega = d^2 k^2 (\hat{e}_s \cdot \hat{e}_z) \Rightarrow \omega = (V_A^2/\omega_c) k^2 (\hat{e}_s \cdot \hat{e}_z), \quad (6.24)$$

and the cyclotron mode

$$\omega = -1(\hat{e}_s \cdot \hat{e}_z) \Rightarrow \omega = -\omega_c(\hat{e}_s \cdot \hat{e}_z), \quad (6.25)$$

respectively. These results represent the exact solutions of the incompressible HMHD [40]. In this limit the amplitudes [related through equations Eqs. (6.14a)-(6.14c)], become

$$A_+ \approx \frac{\alpha}{1 - \alpha k} q \quad ; \quad A_- = \alpha q. \quad (6.26)$$

Therefore the respective relationships for the fluctuating fields, at small  $k$ , are

$$\mathbf{v}_+ = \pm \frac{d}{\sqrt{1 + d^2}} \mathbf{b} = \mathbf{v}_-. \quad (6.27)$$

At large  $k$ , however, the amplitudes for the Whistler mode ( $\alpha = -kd^2$ ) are

$$\mathbf{v}_+ \approx -\mathbf{b}/k \rightarrow 0; \quad \mathbf{v}_- = -kd^2 \mathbf{b}. \quad (6.28)$$

They still remain aligned reflecting the nature of the exact solutions, but their magnitudes differ.

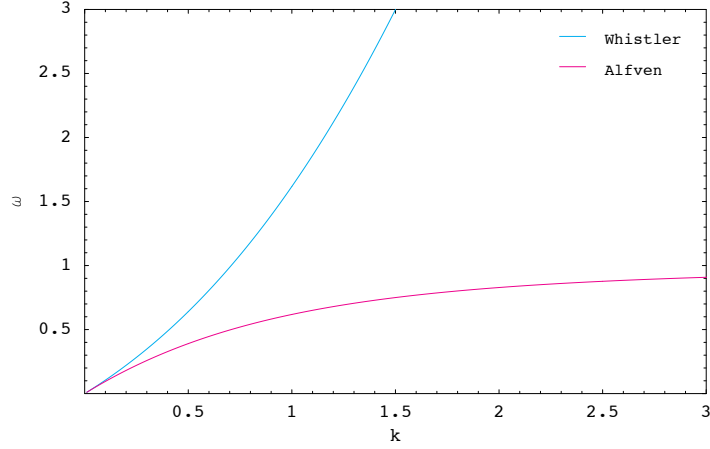


Figure 6.1: Dispersion curves: non-relativistic case ( $V_A \ll c$ ). Note the cyclotron branch (large  $k$ ) asymptotic to 1, or  $\omega_c$  in physical units.

### 6.3.1.2 Relativistic case ( $A_+^2 \lesssim 1$ )

The relativistic version of Fig. 6.1 is shown on shown in Figs. 6.2-6.3. Figure 6.2 shows the frequency of the shear Alfvén mode (asymptoted to the cyclotron branch) as a function of the fluid velocity’s amplitude ( $A_+$ ); the frequency decreases as the amplitude increases. We can understand this analytically by going to the large  $k$  regime, but first let us rewrite Eqs. (6.14a)-(6.14c) using  $\omega = -\alpha k(\hat{e}_s \cdot \hat{e}_z)$

$$-\frac{A_+(\hat{e}_s \cdot \hat{e}_z)k}{\omega} = q + kA_+\gamma_+ \quad (6.29a)$$

$$-\frac{A_-(\hat{e}_s \cdot \hat{e}_z)k}{\omega} = q \quad (6.29b)$$

$$k^2 \left(1 - \frac{\omega^2}{k^2}\right) q = \frac{k}{d^2} [A_+\gamma_+ - A_-\gamma_-] . \quad (6.29c)$$

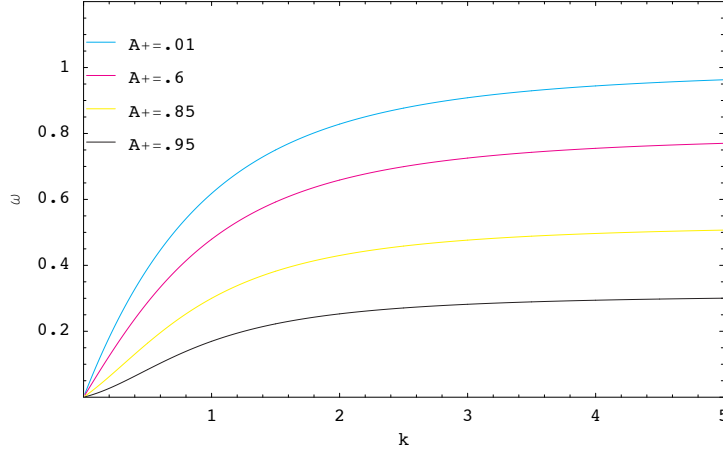


Figure 6.2: Dispersion curves: relativistic case. Alfvénic modes, for various amplitudes  $A_+$ , with  $\hat{e}_s \cdot \hat{e}_z = -1$ .

In the large  $k$  limit we get from Eq. (6.29b)  $A_- \rightarrow 0$  and from Eq. (6.29a)

$$-\frac{A_+(\hat{e}_s \cdot \hat{e}_z)}{\omega} = A_+ \gamma_+, \quad (6.30)$$

or

$$\omega = -\sqrt{1 - A_+^2(\hat{e}_s \cdot \hat{e}_z)}. \quad (6.31)$$

This result explains Fig. 6.2, it tells us that, frequency decreases as the amplitude of the fluid velocity increases, Eq. (6.31) is the relativistic version of Eq. (6.25). For antiparallel propagation Eq. (6.31) becomes (in physical units)

$$\omega = \omega_c \sqrt{1 - A_+^2}, \quad (6.32)$$

thus for small amplitudes and small  $k$  the wave behaves Alfvénically, as  $A_+$  increases it brings down the frequency. This behavior is what in fact permeates

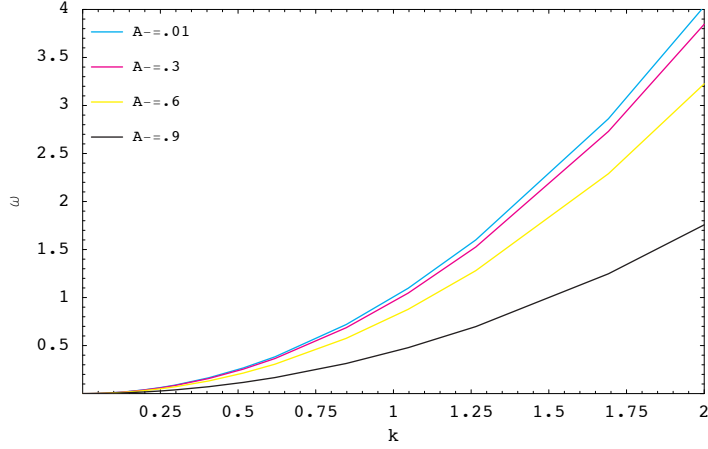


Figure 6.3: Whistler mode for various amplitudes  $A_-$ .

the whole physics of this solutions; there are some exceptions. In general the relativistic nonlinearity in Eq. (6.31) (the  $\gamma_+^{-1}$  factor), boost up the effective mass bringing down the frequency.

Figure 6.3 is another numerical result of Eqs. (6.14a)-(6.14c) and shows that for sufficiently small amplitudes the frequency behaves like the Whistler mode, but as the amplitude is increased, the frequency decreases. To explain this, we note that the Whistler mode is found only in the  $\mathbf{v}_+ \rightarrow 0$  limit of HMHD equations [see Eq. (6.28)]. Therefore to see it we need to set  $A_+ \rightarrow 0$ . Equations. (6.29b) and (6.29c) become

$$-\frac{A_-(\hat{e}_s \cdot \hat{e}_z)k}{\omega} = q \quad (6.33a)$$

$$k^2 \left(1 - 2\frac{\omega^2}{k^2}\right) q = -\frac{k}{d^2} A_- \gamma_- . \quad (6.33b)$$

Solving for  $A_-$  from Eq. (6.33b) and substituting it on Eq. (6.33a) we find,

in the large  $k$  limit,

$$\omega = k^2 d^2 \sqrt{1 - A_-^2 (\hat{e}_s \cdot \hat{e}_z)}, \quad (6.34)$$

the relativistic version of Eq. (6.24). Figure 6.3 shows the plots for the Whistler modes as a function of the amplitude  $A_-$ , with  $(\hat{e}_s \cdot \hat{e}_z) = 1$  (parallel propagation).

### 6.3.1.3 $V_A \gg c$

Another important case is when  $V_A \gg c$ , which we have not studied before. This special case when the Alfvén speed is larger than the speed of light implies a very strong magnetic field. Plots in Fig. 6.4 corresponding to this interesting limit, indicate that the mode is light-like the frequency is essentially independent of the amplitude  $A_+$ , provided that  $V_A$  be sufficiently large. In the non-relativistic limit ( $A_+^2 \ll 1$ ), it is easy to see this behavior. If we use Eq. (6.16), with  $d \gg 1$  and small  $k$ , we obtain

$$[1 - \alpha^2 (\hat{e}_s \cdot \hat{e}_z)^2] \approx 0, \quad (6.35)$$

or

$$\alpha^2 \approx \frac{1}{(\hat{e}_s \cdot \hat{e}_z)^2}. \quad (6.36)$$

This result corresponds to the vacuum dispersion relation since

$$\omega^2 = \alpha^2 k^2 (\hat{e}_s \cdot \hat{e}_z)^2 \Rightarrow \omega^2 = c^2 k^2. \quad (6.37)$$

Note, that in this case, the dispersion relation is independent of the product  $\hat{e}_s \cdot \hat{e}_z$ . Therefore this result is valid for any direction of propagation, parallel, antiparallel, perpendicular or oblique.

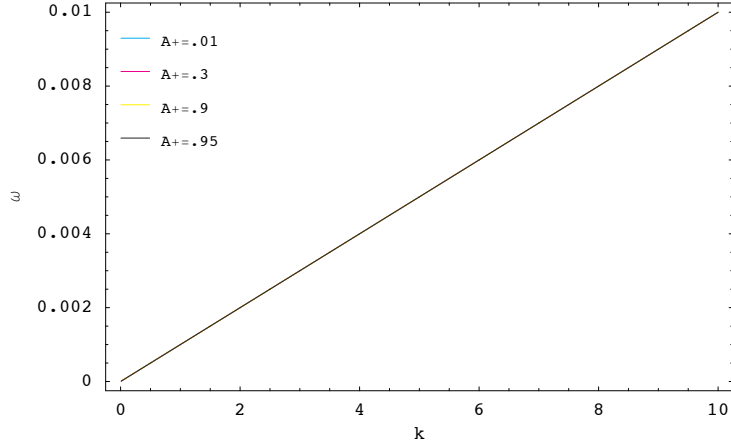


Figure 6.4: Vacuum dispersion relations for different velocity amplitudes ( $V_A \gg c$ ).

In the relativistic limit, Eq. (6.37), still applies according to Fig. 6.4. This is easy to understand, if we take the limit  $d^2 \rightarrow \infty$  of Eq. (6.29c) we obtain

$$k^2 \left( 1 - \frac{\omega^2}{k^2} \right) q = 0 \Rightarrow \omega^2 = k^2. \quad (6.38)$$

Reproducing again the vacuum dispersion relation.

### 6.3.2 Same species $\mu_+ = \mu_- \rightarrow 1/2$

The case when the plasma have species with equal masses and same absolute charges could represent, for example, an electron-positron ( $e^-e^+$ ) plasma. Indeed,  $e^-e^+$  are an example of a larger class of equal mass plasmas or Pair plasmas. Theoretical studies in  $e^-e^+$  plasmas have focused, largely, on the relativistic regime (see Chapter 4). However, here we treat the pair

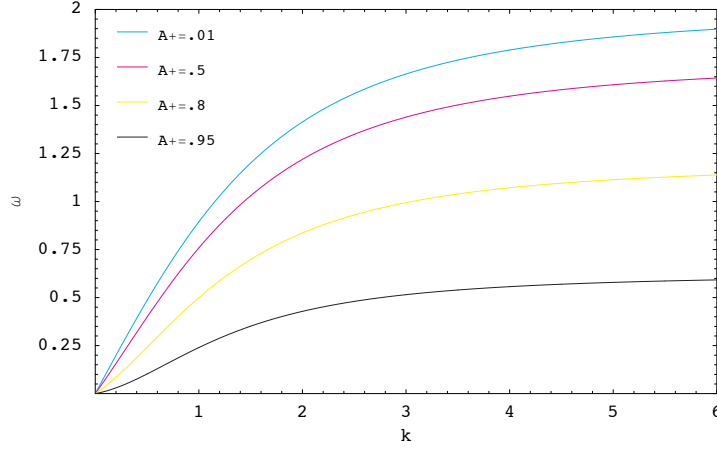


Figure 6.5: Alfvénic modes in pair plasmas, note the asymptotic limit of 2, at large  $k$ .

plasma in the non-relativistic regime as well as in the relativistic regime.

### 6.3.2.1 Non-relativistic case ( $A_+^2 \ll 1$ )

Figure 6.5 (top curve) shows the results for this case, this is the shear Alfvén mode. The difference, between this and the different species case, is that the asymptotic frequency is  $2\omega_c$ , twice as large as the frequency in plasmas where the mass of one species is negligible (electron-ion). This fact may be seen from Eq. (6.15) written in the pair plasma limit

$$(1 - \alpha^2) \left( 1 - \frac{\alpha^2 k^2}{4} \right) = \frac{\alpha^2}{d^2} \quad (6.39)$$

In the small  $k$  limit, Eq. (6.39) gives

$$\alpha = \pm \frac{d}{\sqrt{1 + d^2}}, \quad (6.40)$$

which, after using  $\omega = -\alpha k(\hat{e}_s \cdot \hat{e}_z)$ , gives

$$\omega = \pm \frac{V_A/c}{\sqrt{1 + (V_A/c)^2}} k(\hat{e}_s \cdot \hat{e}_z) \quad (6.41)$$

reproducing the Alfvénic dispersion relation. On the other hand, in the large  $k$  and large  $d$  limit, Eq. (6.39) gives

$$\alpha^2 = \frac{4}{k^2} \Rightarrow \alpha = \pm \frac{2}{k}, \quad (6.42)$$

or

$$\omega = \mp 2\omega_c(\hat{e}_s \cdot \hat{e}_z) \quad (6.43)$$

the cyclotron frequency branch. Note that in this large  $k$  limit, due to the equality in masses, the Whistler mode is not present.

Equation (6.39) also allows the solution, in the limits: large  $k$  and small  $d$

$$\frac{-1}{4}(1 - \alpha^2) \approx \frac{1}{d^2 k^2} \Rightarrow \alpha^2 = \frac{4}{d^2 k^2} + 1, \quad (6.44)$$

or

$$\omega^2 = \frac{4}{d^2} + k^2 \Rightarrow \omega^2 = 4\omega_p^2 + k^2 c^2 \quad (6.45)$$

the plasma electromagnetic mode, see Fig. 6.6.

### 6.3.2.2 Relativistic case ( $A_+^2 \lesssim 1$ )

As shown in Fig. 6.5 we expect the decreasing of frequency with the increasing in amplitude. The analytical expression, derived with the help of Eq. (6.14a) and  $\omega = -\alpha k(\hat{e}_s \cdot \hat{e}_z)$ , explicitly displays this behavior

$$\frac{A_+(\hat{e}_s \cdot \hat{e}_z)k}{\omega} = q + \frac{1}{2}kA_+\gamma_+, \quad (6.46)$$

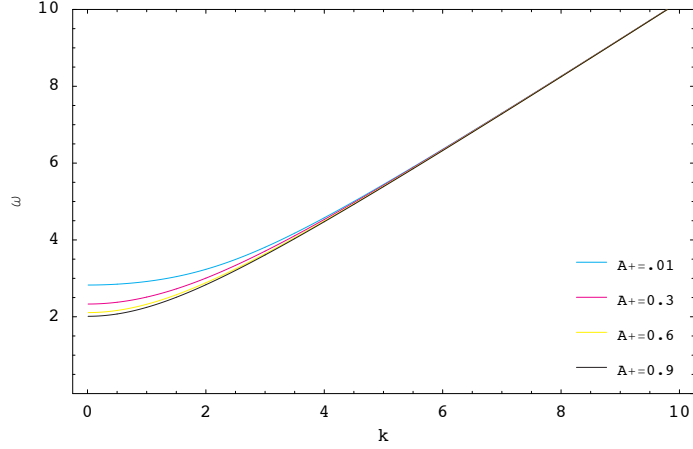


Figure 6.6: Electromagnetic plasma modes for various velocity amplitudes.

which, in the large  $k$ , limit gives the usual resonance frequency (see Fig. 6.5)

$$\omega = -\frac{2\omega_c}{\gamma_+}(\hat{e}_s \cdot \hat{e}_z) \quad (6.47)$$

which decreases with increasing  $\gamma_+$ .

### 6.3.2.3 Case $V_A \gg c$

In this case, the dispersion relation obtained is that of vacuum, as seen in Fig. 6.7. The explanation can be seen from Eq. (6.29c), that still applies in this pair plasma limit,

$$k^2 \left(1 - \frac{\omega^2}{k^2}\right) q = \frac{k}{d^2} [A_+ \gamma_+ - A_- \gamma_-], \quad (6.48)$$

which after taking the  $d \rightarrow \infty$  yields

$$\omega^2 = k^2 c^2. \quad (6.49)$$

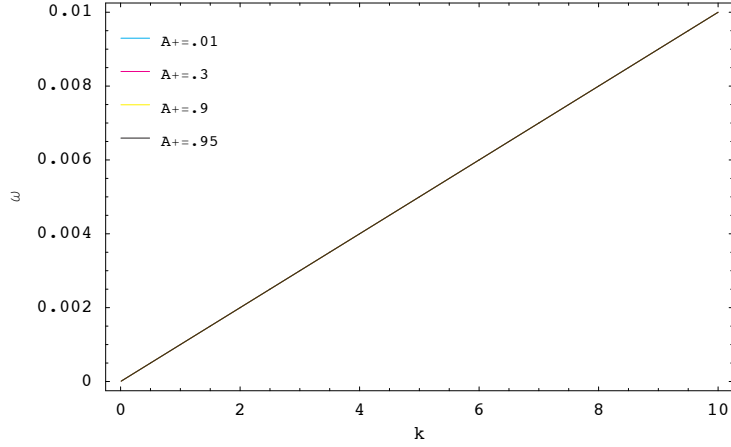


Figure 6.7: Vacuum dispersion relation in pair plasma, limit  $V_A \gg c$ . Note that the curve is unaffected by the increasing amplitude  $A_+$ .

## 6.4 Conclusions

Our results show that in most cases the frequency of the modes decreases as the fluid becomes relativistic. However, despite the decreasing in frequency nonlinear wave properties up to relativistic speeds, for example,  $\sim 0.95 c$ . The decreasing frequency behavior confirms previous results [41], although in Ref. [41] the analysis is limited on  $V_A \sim c$ ; therefore in this work the result is generalized.

Only when the Alfvén speed is much larger than the speed of light (strong magnetized plasma), the modes are not totally affected, behaving light-like even in the ultra-relativistic limit.

The relationship between the amplitudes,  $\mathbf{v}_\pm$  and  $\mathbf{b}$ , is given by Eqs. (6.14a)-(6.14c). They are always aligned, however, only in few cases it is

possible to derive the exact relationship between them, see Eq. (6.26).

In the pair plasma case our results show that there is no Whistler mode. This result, owing to the vanishing of the Hall current, is consistent with earlier work ([34]-[35]).

Exact solutions provide a basis for quantitative models of turbulence, we just hope that these solutions could offer a starting point further in the investigations of turbulent fluctuations.

# Chapter 7

## Summary

In this work we have studied the propagation and stability of waves in astrophysical plasmas. The motivation for the first part, composed of Chapters 3-5, has been:

- To understand the temperature effects on the propagation and stability of waves in pulsar pair plasmas, particularly, the possible stabilization of the two-stream unstable Alfvén wave by relativistic temperatures.
- Explain some of the properties of the radio pulses emanating from pulsars such as frequency and luminosity.

The first task of this dissertation, as we have explain in the introduction, is the study of relativistic waves in pulsar pair plasmas at temperatures of the order of  $T \sim mc^2/k_B$ . At this large temperatures the plasma supports: four modes for parallel propagation, one for perpendicular propagation and four modes for oblique propagation. The modes propagating along the magnetic field lines (parallel propagation) are obviously the most important candidates for explaining the radio emission properties from pulsars, since the emitted radiation is contained in a small narrow region above the polar caps of neutron stars.

Of the four parallel propagating modes, two are electromagnetic plasmas modes and the other two are Alfvénic modes. At large relativistic temperatures, the electromagnetic plasmas modes are affected in the long wavelength region only.

Of the Alfvénic modes, the fast mode is super-luminous for large wavelengths (short  $k$ ), becoming sub-luminous at large  $k$ . In the case of high relativistic temperatures, the super-luminous region reduces to even shorter  $k$ . The slow Alfvén mode, on the other hand, is unstable at large wavelengths and remains so in the case of large relativistic temperatures. This last result is crucial for the free electron laser (FEL) mechanism emphasized in this work.

We have shown that the Alfvénic two-stream instability is unaffected as the temperature rises to levels of  $T \sim mc^2/k_B$ . We have also shown that, for typical values, this instability is faster than the rotational period of the pulsar and therefore has the potential to be a candidate as a possible source of a nonlinear secondary process that could generate coherent radiation.

We, then, go on to show that the interaction of the Alfvénic two-stream instability with the pulsar primary beam could simulate an FEL-like effect given coherent radiation. The predicted range of radiated frequencies and the associated power luminosities are within the range of the observational values obtained from real pulsars. This agreement lends evidence to the dissertation that an FEL-like radiation effect could be responsible for the radio wave pulses emanating from pulsars.

We expect that the specific problems studied in this work, should give a better understanding for the theory of propagating waves in pulsars plasmas and on the radiation mechanisms that produce the pulses. Still more detailed work needs to be done before one can claim that an FEL mechanism is really responsible for the pulsar emissions.

In the second part, composed of Chapter 6, we have studied nonlinear wave solutions in plasmas with arbitrary species mass. We have carried out studies in both the relativistic and in the non-relativistic limit. The solutions found in the different species case are generalizations of the HMHD wave-like solutions.

Our results indicate a decreasing in the frequencies of the Whistler and Alfvén modes as the wave amplitude (effective mass) increases. However, the overall shape of the predicted modes is conserved in most cases.

In the limit of super strong magnetic fields we find that the light-like modes are unaffected by the wave amplitude (relativistic effects).

## Appendix

## Exact solutions to the incompressible MHD

If the dissipative effects are ignored the MHD equations that governed the variations of  $\mathbf{u}$  and  $\mathbf{B}$  are:

$$\frac{\partial \mathbf{B}}{\partial t} = \nabla \times (\mathbf{u} \times \mathbf{B}), \quad (1a)$$

$$\rho \frac{D}{Dt} \mathbf{u} = -\nabla P + \frac{1}{4\pi} (\nabla \times \mathbf{B}) \times \mathbf{B}, \quad (1b)$$

where  $D/Dt = \partial/\partial t + \mathbf{u} \cdot \nabla$  is the co-moving operator. The **standard** procedure to obtain solutions to the above equations is to expand the fields around some equilibrium conditions where the perturbed quantities are **small**, i.e.

$$\mathbf{B} = \mathbf{B}_o + \mathbf{b}, \quad (2)$$

$$\mathbf{u} = \mathbf{v}, \quad (3)$$

where  $\mathbf{B}_o$  is the ambient magnetic field assumed to be uniform, there is no ambient flow. If we do this then Eqs. (1a)-(1b) become:

$$\frac{\partial \mathbf{b}}{\partial t} = \nabla \times [\mathbf{v} \times (\mathbf{B}_o + \mathbf{b})], \quad (4a)$$

$$\rho \frac{D\mathbf{v}}{Dt} = -\nabla P + \frac{1}{4\pi} (\nabla \times \mathbf{b}) \times (\mathbf{B}_o + \mathbf{b}), \quad (4b)$$

the standard approximation is carry out by neglecting the squares and products of the small quantities  $\mathbf{b}$  and  $\mathbf{v}$ , i.e. by making them linear. Then since  $\mathbf{B}_o$  is uniform and  $\nabla \cdot \mathbf{b} = \nabla \cdot \mathbf{v} = 0$ , the Eqs. (4a)-(4b) reduce to:

$$\frac{\partial}{\partial t} \mathbf{b} = (\mathbf{B}_o \cdot \nabla) \mathbf{v}, \quad (5a)$$

$$\rho \frac{\partial}{\partial t} \mathbf{v} = \frac{1}{4\pi} (\mathbf{B}_o \cdot \nabla) \mathbf{b}, \quad (5b)$$

where  $P + \mathbf{B}_o \cdot \mathbf{b}/4\pi = \text{const.}$  For simplicity take the  $z$  direction parallel to  $\mathbf{B}_o$  then Eqs. (5a)-(5b) become:

$$\frac{\partial \mathbf{b}}{\partial t} = B_o \frac{\partial \mathbf{v}}{\partial z}, \quad (6)$$

$$\rho \frac{\partial \mathbf{v}}{\partial t} = \frac{B_o}{4\pi} \frac{\partial \mathbf{b}}{\partial z}, \quad (7)$$

yielding

$$\frac{\partial^2}{\partial t^2} \mathbf{b} = V_A^2 \frac{\partial^2}{\partial z^2} \mathbf{v}, \quad (8a)$$

$$\frac{\partial^2}{\partial t^2} \mathbf{v} = V_A^2 \frac{\partial^2}{\partial z^2} \mathbf{b}, \quad (8b)$$

where  $V_A = B_o/\sqrt{4\pi\rho}$ , as usual.

The **exact solutions** are derived without any approximations about the perturbed quantities, their magnitudes can be as large as one wishes by noting that if  $\mathbf{v}$  and  $\mathbf{b}$  are parallel (or antiparallel) then the term  $\mathbf{v} \times \mathbf{b}$  in Eq. (4a) vanishes exactly, recovering Eq. (5a). Also in Eq. (4b)

$$\frac{1}{4\pi} (\nabla \times \mathbf{b}) \times \mathbf{b} = \frac{1}{4\pi} (\mathbf{b} \cdot \nabla) \mathbf{b} - \nabla \frac{b^2}{8\pi}, \quad (9)$$

therefore Eq. (4b) becomes:

$$\rho \frac{\partial \mathbf{v}}{\partial t} + \rho (\mathbf{v} \cdot \nabla) \mathbf{v} = \frac{1}{4\pi} (\mathbf{B}_o \cdot \nabla) \mathbf{b} - \nabla (P + \mathbf{B}_o \cdot \mathbf{b}/4\pi) + \frac{1}{4\pi} (\mathbf{b} \cdot \nabla) \mathbf{b} - \nabla \frac{b^2}{8\pi}. \quad (10)$$

Now choose

$$\mathbf{v} = \alpha \mathbf{b},$$

where  $\alpha = V_A/B_o$ . Then in Eq. (10), the term  $(\mathbf{b} \cdot \nabla) \mathbf{b}/4\pi$  exactly balances the term  $\rho (\mathbf{v} \cdot \nabla) \mathbf{v}$  to the left, the term  $-\nabla b^2/8\pi$  can be balanced by increasing

the pressure, so that now  $P + \mathbf{B}_o \cdot \mathbf{b}/4\pi + b^2/8\pi$  is a constant. Thus in this case Eq. (10) reduces exactly to the form of Eq. (5b), without any approximation being needed. Therefore it is unnecessary to suppose  $\mathbf{b}$  and  $\mathbf{v}$  to be small quantities whose products are negligible. Thus waves of this type can exist in which  $\mathbf{b}$  is as large as the ambient field  $\mathbf{B}_o$ .

## Bibliography

- [1] R. D. Hazeltine and F. Waelbroeck. *The Framework of Plasma Physics*. Westview Press, 2004.
- [2] L. Tonks and I. Langmuir. *Phys. Rev.*, **33**:1995, 1929.
- [3] D. R. Hartree. *Proc. Camb. Phil. Soc.*, **27**:143, 1931.
- [4] E. V. Appleton. *J. Inst. Elec. Engrs.*, **71**:642, 1932.
- [5] H. Alfvén. *Arkiv. Mat. Astron. Fysik*, **29 B**:2, 1942.
- [6] M. W. Verdon and D. B. Melrose. *Phys. Rev. E*, **77**:046403, 2008.
- [7] P. N. Arendt and J. A. Eilek. *Astrophys. J.*, **581**:451, 2002.
- [8] J. Arons and J. J. Barnard. *Astrophys. J.*, **302**:120, 1986.
- [9] D. B. Melrose. *Plasma Phys. Controlled Fusion*, **39**:A93, 1997.
- [10] M. Gedalin, D. B. Melrose, and E. Gruman. *Phys. Rev. E*, **57**:3399, 1998.
- [11] M. Lyutikov. *Mon. Not. R. Astron. Soc.*, **293**:447, 1998.
- [12] M. Gedalin, E. Gruman, and D. B. Melrose. *Mon. Not. R. Astron. Soc.*, **325**:715, 2001.

- [13] A. Hewish et al. *Nature*, **217**:709, 1968.
- [14] A. G. Lyne and F. Graham-Smith. *Pulsar Astronomy*. Cambridge University Press, 1998.
- [15] J. P. Ostriker. *Nature*, **217**:1227, 1968.
- [16] F. Pacini. *Nature*, **216**:567, 1967.
- [17] T. Gold. *Nature*, **218**:731, 1968.
- [18] W. Baade and F. Zwicky. *Proc. Nat. Acad. Sci.*, **20**:254, 1934.
- [19] J. R. Oppenheimer and G. Volkoff. *Phys. Rev.*, **55**:374, 1939.
- [20] V. S. Beskin, A. V. Gurevich, and Ya. N. Istomin. *Physics of the Pulsar Magnetosphere*. Cambridge University Press, 1993.
- [21] D. Lorimer and M. Kramer. *Handbook of Pulsar Astronomy*. Cambridge University Press, 2005.
- [22] L. D. Landau and E. M. Lifshitz. *The classical theory of fields*. Pergamon Press, Oxford, 1987.
- [23] R. N. Manchester and J. H. Taylor. *Pulsars*. W. H. Freeman and Company, San Francisco, 1977.
- [24] S. M. Mahajan. *Phys. Rev. Lett.*, **90**:035001, 2003.
- [25] V. I. Berezhiani et al. *Phys. Rev. E*, **65**:04702, 2002.

- [26] V. I. Berezhiani and S. M. Mahajan. *Phys. Rev. E*, **52**:1968, 1995.
- [27] V. I. Berezhiani and S. M. Mahajan. *Phys. Rev. Lett.*, **73**:1110, 1994.
- [28] P. Goldreich and W. H. Julian. *Astrophys. J.*, **157**, 1969.
- [29] P. A. Sturrock. *Astrophys. J.*, **164**:529, 1991.
- [30] M. A. Ruderman and P. G. Sutherland. *Astrophys. J.*, **196**:51, 1975.
- [31] D. B. Melrose. *J. Astrophys. Astron.*, **16**:137, 1995.
- [32] A. F. Cheng and M. A. Ruderman. *Astrophys. J.*, **212**:800, 1977.
- [33] A. R. Soto-Chavez et al. *Phys. Rev. E*, **81**:026403, 2010.
- [34] G. P. Zank and R. G. Greaves. *Phys. Rev. E*, **51**:6079, 1995.
- [35] N. Iwamoto. *Phys. Rev. E*, **47**:604, 1993.
- [36] D. Shapakhidze et al. *Phys. Rev. E*, **67**:026407, 2003.
- [37] G. B. Rybicki and A. P. Lightman. *Radiative Processes in Astrophysics*. John Wiley & Sons Inc., 1985.
- [38] P. Luchini and H. Motz. *Undulators and Free-electron lasers*. Oxford University Press, 1990.
- [39] P. J. Coleman Jr. *Phys. Rev. Lett.*, **17**:207, 1962.
- [40] S. M. Mahajan and V. Krishan. *Mon. Not. R. Astron. Soc.*, L1, 2005.
- [41] T. Hada, S. Matsukiyo, and V. Munoz. *arXiv: physics*, 0410203, 2004.

# Index

- Abstract*, vii
- Acknowledgments*, v
- Appendices*, 98
  
- Bibliography*, 104
  
- Dedication*, iv
- density
  - co-rotating, 22
- dispersion relation, 32
  
- energy-momentum tensor, 15
- enthalpy, 16
- Exact solutions*, 78
- Exact solutions to MHD*, 99
  
- Free Electron Lasers (FEL)*, 58
- frequency
  - FEL, 68
  
- instability
  - cyclotron two-stream, 43
  - growth rate, 43
- Introduction*, 1
  
- magnetic field
  - critical, 26
- Maxwellian
  - relativistic, 15
- Model
  - relativistic fluid, 15
- Model*, 15
  
- neutron stars, 7
  
- Physics of Pulsars*, 19
  
- plasma, 1
  - parameters, 1
  - relativistic, 1
- pulsar plasmas, 3
  - relativistic waves, 30
  - streaming, 28
  - temperature, 29
- pulsars, 4
  - brightness temperature, 13
  - flux density, 10
  - lighthouse effect, 7
  - luminosity, 13
  - magnetic field, 9
  - magnetosphere, 19
    - FEL in, 72
  - light cylinder, 22
  - moment of inertia, 8
  - polar cap, 24
  - radiation, 59
  - spin-down energy, 8
  
- radiation
  - curvature, 26
- Relativistic Waves*, 30
  
- Summary*, 95
  
- vorticity, 17

## Vita

Angel Rualdo Soto Chavez was born in Guatemala, the son of Rualdo Soto and Blanca Chavez. He received the Bachelor of Science degree in Engineering from the Universidad de San Carlos de Guatemala. Later he earned his Master of Science (Diploma) from the International Center for Theoretical Physics in Trieste Italy. He later applied to The University of Texas at Austin for enrollment in its physics program where he became a PhD candidate. He is happily married and has one son.

Permanent address: rualdo\_sotochavez@yahoo.com

This dissertation was typeset with  $\text{\LaTeX}^\dagger$  by the author.

---

<sup>†</sup> $\text{\LaTeX}$  is a document preparation system developed by Leslie Lamport as a special version of Donald Knuth's  $\text{\TeX}$  Program.